

Addressing Imperfect Symmetry: a Novel Symmetry-Learning Actor-Critic Extension

Miguel Abreu, Luis Paulo Reis, and Nuno Lau

Abstract—Symmetry, a fundamental concept to understand our environment, often oversimplifies reality from a mathematical perspective. Humans are a prime example, deviating from perfect symmetry in terms of appearance and cognitive biases (e.g. having a dominant hand). Nevertheless, our brain can easily overcome these imperfections and efficiently adapt to symmetrical tasks. The driving motivation behind this work lies in capturing this ability through reinforcement learning. To this end, we introduce Adaptive Symmetry Learning (ASL) — a model-minimization actor-critic extension that addresses incomplete or inexact symmetry descriptions by adapting itself during the learning process. ASL consists of a symmetry fitting component and a modular loss function that enforces a common symmetric relation across all states while adapting to the learned policy. The performance of ASL is compared to existing symmetry-enhanced methods in a case study involving a four-legged ant model for multidirectional locomotion tasks. The results demonstrate that ASL is capable of recovering from large perturbations and generalizing knowledge to hidden symmetric states. It achieves comparable or better performance than alternative methods in most scenarios, making it a valuable approach for leveraging model symmetry while compensating for inherent perturbations.

I. INTRODUCTION

SYMMETRY is a multidisciplinary concept that plays a fundamental role in how we perceive the world, from abstract beauty and harmony, up to precise definitions in physics, biology, mathematics, and many other disciplines. In the scope of this paper, symmetry is studied through geometry, and, more precisely, group theory. Weyl [1] takes a top-down approach to define symmetry, starting with a vague notion of proportion and balance, then delving into the intuitive notion of reflections and rotations, and ending with the characterization of invariance with respect to a group of automorphisms (i.e. mappings of a mathematical object onto itself that preserve the structure of space).

Weyl acknowledges that in reality, the actual group of automorphisms may be unknown, leading researchers to narrow the invariant conditions, for a precise analysis to be possible. In the context of this paper, let us start with a biology example that doubles as motivation. Consider the act of throwing a crumpled paper into a bin at a reasonable distance. Assume a

bilaterally symmetrical non-ambidextrous human. The dominant arm/hand will easily find several trajectories for the paper to reach the bin and, with enough training, the other arm will be able to find equivalent mirrored trajectories.

This means that the human brain is able to learn how to compensate for internal imbalances to produce a symmetric outcome. Internal imbalances include differences in arm strength, weight and other physical attributes, as well as handedness and other cognitive biases. Additionally, the brain may also have to compensate for external factors, e.g. wearing a thick glove on the left hand.

A. Symmetry Perturbations

These symmetry perturbations do not imply an asymmetric relation between both actions. Assume the human's initial state s_0 is a bilaterally symmetrical pose. The motor cortex generates muscle contractions by producing neural activity patterns. The patterns that result in throwing with the dominant arm/hand represent action a_d , while the patterns that deal with the other arm represent action a_z . There might be a map $g_{s_0} : \mathcal{A}_{s_0} \rightarrow \mathcal{A}_{s_0}$, where, in state s_0 , for every action $a_d \in \mathcal{A}_{s_0}$ there is an action $a_z \in \mathcal{A}_{s_0}$ that results in a symmetric outcome, where \mathcal{A}_{s_0} is a group of symmetrizable actions in state s_0 . In this context, actions are not symmetrizable when, for instance, a shorter arm cannot perform the same role as a longer arm.

When the map's estimate \hat{g}_{s_0} is a simplification of the ground truth, we say that the symmetry description it provides is incomplete or inexact. Symmetry perturbation, hereinafter referred to simply as perturbation, is any factor that stands between \hat{g}_{s_0} and g_{s_0} , affecting the mapping between pairs of symmetric actions, i.e., actions that lead to two symmetric states when applied to the same initial state. Note that this analysis only makes sense for state-action pairs, as the invariance that characterizes symmetric actions concerns the state that follows. These notions will be formalized in Section II, while defining Markov Decision Processes and their homomorphisms.

Despite the search of symmetry for aesthetic or functional purposes, our brain has evolved to be asymmetric [2], both in terms of specialized regions and motor skills. About 9.33% of humans are mixed-handed, while only around 1% or 2% are ambidextrous, depending on the classification criteria [3]. Symmetry might not always mean better performance, and this uncertainty must be taken into account. Translating this concept to reinforcement learning (RL), it would mean that symmetry should guide the learning process, but never to the detriment of the primary optimization objective.

The first author is supported by FCT — Foundation for Science and Technology under grant SFRH/BD/139926/2018. This work was financially supported by FCT/MCTES (PIDDAC), under projects UIDB/00027/2020 (LIACC) and UIDB/00127/2020 (IEETA).

Miguel Abreu and Luis Paulo Reis are with LIACC/LASI/FEUP, Artificial Intelligence and Computer Science Laboratory, Faculty of Engineering, University of Porto, Porto, Portugal.

Nuno Lau is with IEETA/LASI/DETI, Institute of Electronics and Informatics Engineering of Aveiro, Department of Electronics, Telecommunications and Informatics, University of Aveiro, Aveiro, Portugal.

B. Model Minimization

This paper presents a case study of a four-legged ant model with a total order of symmetry of 8, used to learn multi-directional locomotion tasks under the influence of multiple symmetry perturbations. The robot’s symmetry group includes 4 planes of symmetry and 4-fold rotational symmetry, where one rotation is an identity operation, resulting in 7 non-identity transformations. This is a challenging task, where finding a good policy in an efficient way heavily depends on how the learning algorithm explores the symmetry group.

Most symmetry leveraging techniques fall within temporal or spatial domains. The former, which pertains to invariability under temporal transformations, such as scaling or inversion, is relatively uncommon in robotic tasks. Techniques centered around spatial symmetry are more prevalent, and can be divided into multiple areas, as described in following paragraphs.

1) *Relabeling states and actions*: The first spatial symmetry technique concerns the permutation of roles of equivariant parts in the state and action spaces. For instance, consider a bilaterally symmetrical robot that throws a ball with one arm, while stabilizing itself with the other. The policy could learn independent actions for a left throw and a right throw. However, it could abstract the side by just considering a *throwing arm* and a *stabilizing arm*. The user just has to relabel both arms when assigning the state, depending on the preferred throwing side for the next episode. After the policy computes an action, the user has to relabel them again to assign the resulting action correctly to both arms. This approach can be implemented directly in the simulator without requiring modifications to the optimization algorithm.

2) *Data augmentation*: Data augmentation is commonly used in RL to enhance sample efficiency and stability, being experience replay, introduced by Lin [4], one of its main precursors. In the scope of this work, data augmentation involves the creation of symmetric copies of real experiences. Using the last example, after the robot threw the ball with its left arm, the RL algorithm would also receive artificially created samples of the same experience, but executed with the right arm. Ultimately, there is twice as much information to learn from.

3) *Symmetric Networks*: This approach enforces symmetry constraints directly on the policy, by modifying the network architecture. In domains where symmetry is a requirement of optimal solutions, this is a robust method. However, this assumption cannot be made for many robotic tasks, including locomotion, where it is unclear whether perfect symmetry is mechanically preferable. Real robots exhibit imperfections like humans, who learn to compensate for asymmetries and perceive the resulting gaits as normal or unimpaired [5], [6].

4) *Symmetry Loss Function*: In optimization problems, a loss function quantifies the cost of an event. In RL, this function is responsible for maximizing a cumulative reward over time, while also sustainably guiding the learning process. In the ball throwing robot example, the reward could measure how close the ball is to the target. Also, if symmetry was desired, it could be added to the reward as a scalar value, but there is a better alternative.

A reward is useful when evaluating a metric that requires interaction with the environment. Symmetry does not have such limitation, as its compliance can be measured through analytical functions that take the policy as input. By incorporating this knowledge into the primary loss function, the algorithm is able to steer the policy’s parameters in the right direction through a gradient.

Despite not providing symmetry guarantees, like the relabeling method or symmetric networks, a loss function is the most flexible approach, both at design and runtime stages. It allows users to dynamically regulate the importance of symmetry and fine-tune the learning process. However, current contributions fall short in addressing symmetry perturbations. To bridge this gap, our work introduces a novel approach to leverage model symmetry, while learning and compensating for symmetry perturbations in the system.

The main contributions of this work can be summarized as:

- 1) We introduce Adaptive Symmetry Learning (ASL) ¹ — a model-minimization actor-critic extension that is able to handle incomplete or inexact symmetry descriptions by adapting itself during the learning process;
- 2) ASL is composed of two parts — symmetry fitting, described above; and a new loss function, capable of applying the learned descriptions based on their importance, while actively avoiding neutral states and disadvantageous updates;
- 3) We propose modifications to two existing symmetry loss functions — MSL [30] and PSL [31] — extending them with value losses and the capacity to handle involutory transformations, such as most rotations;
- 4) We present the case study of an ant robot, where we compare the performance of MSL, PSL, ASL, and vanilla PPO [39] in a set of ant locomotion scenarios. We test controlled and realistic symmetry perturbations, as well as partial goal observation, where the policy must discover the best symmetric gait without exploring the symmetric side, while acknowledging the existence of perturbations.

II. PRELIMINARIES

Typical reinforcement learning problems can be described as a Markov Decision Process (MDP) – a tuple $\langle \mathcal{S}, \mathcal{A}, \Psi, p, r \rangle$, with a set of states \mathcal{S} , a set of actions \mathcal{A} , a set of possible state-action pairs $\Psi \subseteq \mathcal{S} \times \mathcal{A}$, a transition function $p(s, a, s') : \Psi \times \mathcal{S} \rightarrow [0, 1]$, and a reward function $r(s, a) : \Psi \rightarrow \mathbb{R}$.

A. MDP transformations

Model reduction allows the exploitation of redundant or symmetric features. To this end, Ravindran and Barto [7] proposed a mathematical formalism to describe MDP homomorphisms — a transformation that groups equivalent states and actions. An MDP homomorphism h from $M = \langle \mathcal{S}, \mathcal{A}, \Psi, p, r \rangle$ to $\check{M} = \langle \check{\mathcal{S}}, \check{\mathcal{A}}, \check{\Psi}, \check{p}, \check{r} \rangle$ can be defined as a surjection $h : \Psi \rightarrow \check{\Psi}$, which is itself defined by a tuple of surjections $\langle f, \{g_s | s \in \mathcal{S}\} \rangle$. In other words, equivalent state-action pairs

¹<https://github.com/m-abr/Adaptive-Symmetry-Learning>

in \tilde{M} are mapped by h to the same abstract state-action pair in \tilde{M} . For $(s, a) \in \Psi$, the surjective function $h((s, a)) = (f(s), g_s(a))$, where $f : \mathcal{S} \rightarrow \tilde{\mathcal{S}}$ and $g_s : \mathcal{A}_s \rightarrow \tilde{\mathcal{A}}_{f(s)}$ for $s \in \mathcal{S}$, satisfies:

$$\check{p}(f(s), g_s(a), f(s')) = \sum_{s'' \in [s']_B} p(s, a, s''), \quad (1)$$

$$\forall s, s' \in \mathcal{S}, a \in \mathcal{A}_s,$$

$$\text{and } \check{r}(f(s), g_s(a)) = r(s, a), \quad \forall s \in \mathcal{S}, a \in \mathcal{A}_s, \quad (2)$$

where B is a partition of \mathcal{S} into equivalence classes, and $[s']_B$ denotes the block of partition B to which state s' belongs.

MDP symmetries constitute a specialization of the described framework, where f and $g_s, s \in \mathcal{S}$ are bijective functions and, consequently, the homomorphism $h = \langle f, \{g_s | s \in \mathcal{S}\} \rangle$ from M to \tilde{M} is an isomorphism. Additionally, since symmetries can be characterized as MDP isomorphisms from and to the same MDP, they are automorphisms, which simplifies the homomorphism conditions (1) and (2):

$$p(f(s), g_s(a), f(s')) = p(s, a, s'), \quad \forall s, s' \in \mathcal{S}, a \in \mathcal{A}_s, \quad (3)$$

$$\text{and } r(f(s), g_s(a)) = r(s, a), \quad \forall s \in \mathcal{S}, a \in \mathcal{A}_s. \quad (4)$$

When referring to $g_s(a)$, the state s corresponding to the state-action pair $(s, a) \in \Psi$ is implicit, and will thus be omitted in the remainder of this document, being the action transformation denoted as $g(a)$. As MDP automorphisms, symmetries can be defined in a single MDP, M . In the aforementioned ball throwing robot example, assume that starting with the ball on the left hand (state s), the robot will perform an optimal left throw (action a). In a mirrored initial state $f(s)$, a mirrored action $g(a)$ is guaranteed to be optimal if all states in Ψ are symmetrizable. Equation (3) holds in this scenario because the probability of ending in an optimal state by performing action a in s is the same as performing $g(a)$ in $f(s)$. As for (4), it also holds, since the reward in both cases should be the same, otherwise it would contain an asymmetric bias.

B. Policy notation

When optimizing a policy π parameterized by θ , the notion of symmetric action has two possible interpretations: $g(a)$, which is the result of mapping a through function g ; and $\pi_\theta(f(s_t))$, which represents the action chosen by the policy for the symmetric state. Frequently, the former is used as a target value for the latter. Stochastic policies that follow a normal distribution $\mathcal{N}(\mu, \sigma)$ are characterized by a mean μ , usually parameterized in RL by a neural network, and a standard deviation σ , optimized independently for exploration. The parameterized mean value μ_θ is particularly useful for symmetry losses, as it represents the current policy without exploration noise, or, more formally, $\mu_\theta(\cdot) = \pi_\theta(\cdot | \sigma = 0)$. Hereinafter, a_t denotes an action sampled from a stochastic policy π_θ at time t , while \bar{a}_t represents the mean of the distribution when a_t was sampled. Extending this notation to the already introduced symmetry mapping yields:

$$\bar{a}_t = \mu_{\theta_{\text{old}}}(s_t), \quad (5)$$

$$\bar{a}'_t = \mu_{\theta_{\text{old}}}(f(s_t)), \quad (6)$$

where θ_{old} means that \bar{a}_t and \bar{a}'_t were obtained from a snapshot of θ and thus are not a function of the current θ . In other words, variables obtained from θ_{old} are constants, not trainable during optimization.

C. Symmetric policy

Zinkevich and Balch [8] define that for a policy to be functionally homogeneous, if $\pi(s) = a$, then $\pi(f(s)) = g(a)$, for all $(s, a) \in \Psi$. When dealing with reflection symmetries, objects are invariant under involutory transformations, i.e., obtaining the symmetric object and the original again just requires applying the same transformation twice. Mathematically, a function f that maps reflection symmetries is an involution ($f = f^{-1}$). In this context, a policy π is symmetric if $\pi(s) = g(\pi(f(s))), \forall s \in \mathcal{S}$.

However, some symmetric transformations, including scaling, rotation and translation cannot always be inverted through the same function. Rotation around an axis, for instance, is only involutory when the transformation angle r in radians is a multiple of π ($r = k\pi, k \in \mathbb{Z}$). For example, if $r = \pi/4$, the previous symmetric policy definition fails because after the state is rotated by $\pi/4$ radians, the action is also rotated by the same angle, not yielding the original action.

Generalizing the symmetric policy definition to noninvolutory transformations only requires changing the side of one operation, such that $g(\pi(s)) = \pi(f(s)), \forall s \in \mathcal{S}$. Care has to be taken when devising symmetry loss functions, to abide by this principle and avoid the negative effect that noninvolutory transformations would otherwise cause.

D. Neutral states

A state s is said to be neutral if it is invariant under f , i.e., $s = f(s)$. Under a symmetric policy, neutral states are inescapable, in the sense that all future states are guaranteed to also be neutral, unless the environment introduces its own bias. This problem occurs in numerous scenarios, from board games to robotic tasks. Consider the problem of a humanoid robot trying to initiate walking by taking its first step, but at the beginning of the episode, the environment is in a neutral state, $s_0 = f(s_0)$. The symmetric policy cannot raise the left foot to take the first step in s_0 because that would mean the right foot should be raised in $f(s_0)$, but this is impossible because there are two actions for the same state and $\pi(s_0) \neq g(\pi(s_0))$. So, one possible option would be to jump with both legs, but after that, it would still be stuck in a neutral state unless the environment introduced some noise.

Perfectly symmetric policies are therefore inadequate for neutral states. Moreover, neighboring states are also affected due to the generalization ability of neural networks and the fact that they represent continuous functions. A solution based on a symmetry exclusion region around neutral states is presented in Section IX-B.

III. RELATED WORK

This section builds upon the model minimization overview from Section I-B and explores specific techniques, along with their advantages and disadvantages. In terms of temporal symmetry, achieving time inversion requires a conservative system without energy loss, such as a frictionless pendulum controlled through RL, as proposed by Agostini and Celaya [9]. However, this assumption is impractical for real-world systems, making this approach less desirable. As for spatial symmetry, the contributions fall into the previously established categories:

1) *Relabeling states and actions*: Zeng and Graham [10] and Ildefonso et al. [11] create symmetry-reduced experiences in actor-critic and value-based domains, respectively, by shrinking the state space, running the policy, and finally restoring the actions using data from the original state. Surovik et al. [12] combine relabeling states and actions with reflection transformations to swap frame-dependent values, such as lateral rotation, to effectively reduce the state volume of a tensegrity robot.

However, this same idea can be applied for robot locomotion with simpler models. If, instead of left and right, we think of "stance" and "non-stance" leg for a biped robot, we can relabel them every half cycle to obtain a symmetric controller [13], [14]. Peng et al. [15] apply this relabeling method at fixed intervals of 0.5 s, forcing a fixed period on the gait cycle. This idea is simple to implement but the policy is constrained by some symmetry switch, whether it is based on time or behavioral pattern.

2) *Data augmentation*: In symmetry oriented solutions, data augmentation can be used with model-based [16] or model-free RL algorithms, although the scope of this work is limited to the latter alternative. Examples of successful applications of this technique include a real dual-armed humanoid robot that moves objects [17], the walking gait of several humanoid models [18] and a quadruped with more than one plane of symmetry [19], among others [9], [20]. If changing the loss function is possible, it is always preferable to data augmentation in terms of computational efficiency and memory footprint, despite the additional initial effort.

3) *Symmetric Network*: Concerning humanoid models, Abdolhosseini et al. [18] introduced a symmetric network architecture that forces perfect symmetry. This method guarantees that if states and actions are symmetrically normalized, the behavior has no asymmetric bias. However, as the authors acknowledge, neutral states are inescapable. Pol et al. [21] generalize this approach to additional problems by introducing MDP homomorphic networks, which can be automatically constructed by stacking equivariant layers through a numerical algorithm. The equivariance constraints (under a group of reflections or rotations) are applied to the policy and value networks. Encoding invariances in neural networks [22]–[26] and the group of network solutions in general lacks the ability to control the symmetry enforcement at runtime and the ability to symmetrize asymmetric models.

4) *Symmetry Loss function*: Mahajan and Tulabandhula [27], [28] proposed an automated symmetry detection process and a method of incorporating that knowledge in

the Q-learning algorithm [29]. A soft constraint was presented as an additional loss for the Q-function approximator, $\hat{\mathbb{E}}_t[(Q_\theta(f(s_t), g(a_t)) - Q_\theta(s, a))^2]$, where θ is the parameter vector of Q , and the expectation $\hat{\mathbb{E}}_t$ indicates the empirical average over a batch of samples. Yu et al. [30] transpose this idea to policy gradients by fusing a new curriculum learning method with an homologous loss function — the Mirror Symmetry Loss (MSL), $\sum_i \|(\pi_\theta(s_i) - g(\pi_\theta(f(s_i))))\|^2$. The authors present very good results when both approaches are used simultaneously.

In previous work, we have presented the Proximal Symmetry Loss (PSL) [31], a loss function aimed at increasing the sample efficiency of the Proximal Policy Optimization (PPO) algorithm [39] by leveraging static model symmetries. The loss function was built to allow asymmetric exploration in models without symmetry perturbations. It leverages the trust region concept to harmonize its behavior with PPO's exploration, which is especially noticeable in smaller batch sizes.

In the next section we will delve into the details of MSL and PSL, while suggesting some modifications to expand the functionality of both loss functions. Then, we introduce the Adaptive Symmetry Learning, with the ability to handle imperfect symmetry by adapting itself during the learning process.

IV. SYMMETRY LOSS FUNCTION

A symmetry loss function computes a value that we seek to minimize in order to obtain a symmetric behavior. Formally, if the robot performs action $a \in \mathcal{A}_s$ in state $s \in \mathcal{S}$, it should also perform the symmetric action $g(a)$ in the symmetric state $f(s)$. Since symmetry is not always the main objective while learning a new behavior, a good symmetry objective function should allow asymmetric exploration in favor of a better policy.

To understand the effect of the proposed loss function, we must analyze the most common implementation of PPO, where the policy and value networks do not share parameters. The PPO's objective L^{PPO} can then be expressed as:

$$L^{PPO}(\theta, \omega) = \hat{\mathbb{E}}_t [L_t^C(\theta) - L_t^{VF}(\omega) + cH(\theta)], \quad (7)$$

$$\text{with } L_t^C(\theta) = \min \left(r_t(\theta) \hat{A}_t, (1 + \text{sgn}(\hat{A}_t)\epsilon) \hat{A}_t \right), \quad (8)$$

$$\text{and } r_t(\theta) = \frac{\pi_\theta(a_t | s_t)}{\pi_{\theta_{old}}(a_t | s_t)}, \quad (9)$$

where the stochastic policy π_θ is parameterized by θ and the value function by ω . $\pi_{\theta_{old}}$ is a copy of the policy before each update, \hat{A}_t is the estimator of the advantage function, L_t^{VF} is a squared error loss to update the value function, ϵ is a clipping parameter, c is a coefficient and H is the policy's distribution entropy. The expectation $\hat{\mathbb{E}}_t$ indicates the empirical average over a finite batch of samples. The main objective of this algorithm is to keep the policy update within a trust region, preventing greedy updates that can be detrimental to learning. This behavior is formalized in the surrogate objective L_t^C , as depicted in Fig. 1 for a single time step.

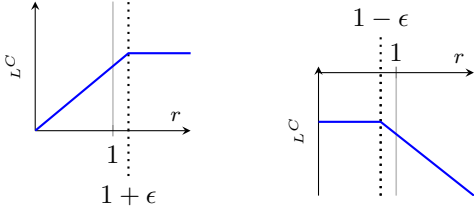


Fig. 1. Plots for PPO's surrogate objective function L^C as a function of ratio r , for a single time step, for a positive advantage estimate (on the left) or a negative advantage estimate (on the right).

A. Extended loss function

PPO's objective L^{PPO} can be extended with an arbitrary symmetry loss L^S , such that

$$L^{PPO+S}(\theta, \omega) = L^{PPO}(\theta, \omega) - L^S(\theta, \omega), \quad (10)$$

$$\text{with } L^S(\theta, \omega) = \hat{\mathbb{E}}_t [w_\pi \cdot L_t^\pi(\theta) + w_V \cdot L_t^V(\omega)], \quad (11)$$

where L_t^π and L_t^V are symmetry loss functions that influence the update gradient of the policy (actor) and value function (critic), respectively.

In L_t^C , the ratio r_t starts at 1 and tends to stay close to that value during optimization. The advantage estimate \hat{A}_t is z-score normalized in typical PPO implementations [32], [33], resulting in a mean of 0. Consequently, L_t^C 's value is usually stable, with a low order of magnitude, which is important to retain when devising extensions, to preserve harmonious interactions among all losses.

B. Generalized Symmetry Loss

The symmetry loss function can be expanded to an arbitrary number of symmetries with minimal changes. Let $j \in \{1, 2, 3, \dots, N\}$ be a symmetry index for a total of N symmetries. Functions $f_j(s)$ and $g_j(a)$ apply symmetry transformation j to state s , and s -dependent action a , respectively. Accordingly, (11) can be rewritten as

$$\begin{aligned} L^S(\theta, \omega) &= \hat{\mathbb{E}}_t [(w_1^\pi \cdot L_{1,t}^\pi(\theta) + w_1^V \cdot L_{1,t}^V(\omega)) + \\ &\quad (w_2^\pi \cdot L_{2,t}^\pi(\theta) + w_2^V \cdot L_{2,t}^V(\omega)) + \\ &\quad \dots + \\ &\quad (w_N^\pi \cdot L_{N,t}^\pi(\theta) + w_N^V \cdot L_{N,t}^V(\omega))] \\ &= \sum_{j=1}^N \hat{\mathbb{E}}_t [w_j^\pi \cdot L_{j,t}^\pi(\theta) + w_j^V \cdot L_{j,t}^V(\omega)] \quad . \quad (12) \end{aligned}$$

V. MIRROR SYMMETRY LOSS

The Mirror Symmetry Loss (MSL) function proposed by Yu et al. [30] $w_\pi \cdot \sum_i \|\mu_\theta(s_t) - g(\mu_\theta(f(s_t)))\|^2$, where w_π is a weight factor, computes the square error between the mean action taken by the stochastic policy before and after the symmetric transformation. On the one hand, this means that after crossing a certain asymmetry threshold, the loss dominates the policy gradient. On the other hand, if that

threshold is crossed to the symmetric side, the symmetry loss loses influence in the policy update. Therefore, w_π does not dictate the weight of the symmetry loss in a consistent way, when computing the gradient, but rather the position of the symmetry threshold. Moreover, since the square error is based on actions, instead of probabilities, the weight of the symmetry loss is also dependent on the action space.

One other problem of this equation is the assumption of involutory transformations, a pitfall introduced in Section II-C. As aforementioned, this issue can be solved by changing where the action transformations is applied. Additionally, the method can be expanded with a value loss, in order to leverage the critic in actor-critic methods. Note that these modifications are a generalization of the original method and do not restrict its previous abilities in any way. The improved mirror symmetry loss function becomes

$$L^{MSL}(\theta, \omega) = \hat{\mathbb{E}}_t [w_\pi \cdot L_t^\pi(\theta) + w_V \cdot L_t^V(\omega)], \quad (13)$$

$$\text{with } L^\pi(\theta) = \hat{\mathbb{E}}_t \|g(\mu_\theta(s_t)) - \mu_\theta(f(s_t))\|^2, \quad (14)$$

$$L^V(\omega) = \hat{\mathbb{E}}_t [(V_\omega(f(s_t)) - V_t^{\text{targ}})^2], \quad (15)$$

where L^π and L^V are the policy and value losses for symmetry, and w^π and w^V are the respective weight factors. The value loss reduces the difference between the value function (for the symmetric state), and the same value target used by PPO.

The generalization in (12) can be applied to MSL by deriving $L_{j,t}^\pi$ and $L_{j,t}^V$ from (14) and (15), respectively,

$$L_{j,t}^\pi(\theta) = \|g_j(\mu_\theta(s_t)) - \mu_\theta(f_j(s_t))\|^2, \quad (16)$$

$$L_{j,t}^V(\omega) = (V_\omega(f_j(s_t)) - V_t^{\text{targ}})^2. \quad (17)$$

VI. PROXIMAL SYMMETRY LOSS

The Proximal Symmetry Loss (PSL) builds on the trust region concept of PPO to reduce the model's asymmetry iteratively [31]. In contrast with MSL, PSL can already handle non-involutory operations. However, it was also generalized in this work to include a value loss component, such that

$$L^{PSL}(\theta, \omega) = \hat{\mathbb{E}}_t [w_\pi \cdot L_t^\pi(\theta) + w_V \cdot L_t^V(\omega)], \quad (18)$$

$$\text{with } L^\pi(\theta) = -\hat{\mathbb{E}}_t [\min(x_t(\theta), 1 + \epsilon)], \quad (19)$$

$$L^V(\omega) = \hat{\mathbb{E}}_t [(V_\omega(f(s_t)) - V_t^{\text{targ}})^2], \quad (20)$$

where ϵ is a clipping parameter shared with L^{PPO} , and x_t is a symmetry probability ratio.

In contrast to (8), L^π does not rely on an advantage estimator to determine the update direction, as its goal is to consistently increase or preserve symmetry. However, the RL algorithm can still opt to decrease symmetry if it benefits the policy, prioritizing L_t^C over L_t^S in (10). Furthermore, although

the symmetry probability ratio shares similarities with (9), there are some distinctions:

$$x_t(\theta) = \frac{\min(\pi_\theta(g(\bar{a}_t) | f(s_t)), \pi_{\theta_{old}}(a_t | s_t))}{\pi_{\theta_{old}}(g(\bar{a}_t) | f(s_t))}, \quad (21)$$

where $\bar{a}_t = \mu_{\theta_{old}}(s_t)$ as defined in (5). Parameters $\pi_\theta(\cdot | s)$ and $\pi_{\theta_{old}}(\cdot | s)$ represent probability distributions during, and before the update, respectively, in accordance with the notation provided in Section II-B. The only term that is not constant during a policy update is $\pi_\theta(g(\bar{a}_t) | f(s_t))$, and only θ is being optimized. Note that θ_{old} is constant because it represents the policy's parameters before the update.

A. Unidirectional update

The policy is modified so that the action $\pi_\theta(f(s_t))$ carried out in the symmetric state $f(s_t)$ becomes symmetric to the action taken in the explored state s_t . Note that ratio x_t in (21) promotes an adjustment to $\pi_\theta(f(s_t))$ without changing $\pi_\theta(s_t)$. In contrast, the mirror symmetry loss attempts to reduce the distance between $\pi_\theta(f(s_t))$ and $\pi_\theta(s_t)$ by promoting changes to both. This approach is generally adequate, except when there are exploration imbalances in symmetric states. One instance is when a humanoid robot is learning how to navigate a maze, but it initially experiences more left turns than right turns.

While exploring left turns, it makes sense to adapt the right turning ability to match the symmetric technique, but not vice versa. Adopting the right turning knowledge to change the left turning skill would be detrimental in this case. Yet, when the robot actually explores right turns, it will try to adapt the symmetric action in the wrong direction, but the effect will be diluted by the low probability of experiencing right turns. In summary, adapting the symmetric action is better than the explored action, because the explored action is more likely to be optimal than the symmetric action. In an extreme case, the symmetric state may be unreachable, making the symmetric action unreliable.

B. Generalized Proximal Symmetry Loss

Similarly to MSL, PSL can also be expanded to an arbitrary number of symmetries by employing (12) and deriving $L_{j,t}^\pi$ and $L_{j,t}^V$, yielding:

$$L_{j,t}^\pi(\theta) = -\min(x_{j,t}(\theta), 1 + \epsilon), \quad (22)$$

$$L_{j,t}^V(\omega) = (V_\omega(f_j(s_t)) - V_t^{\text{targ}})^2, \quad (23)$$

$$\text{with } x_{j,t}(\theta) = \frac{\min(\pi_\theta(g_j(\bar{a}_t) | f_j(s_t)), \pi_{\theta_{old}}(a_t | s_t))}{\pi_{\theta_{old}}(g_j(\bar{a}_t) | f_j(s_t))}. \quad (24)$$

VII. ADAPTIVE SYMMETRY LEARNING: OVERVIEW

The previous symmetry loss functions follow the provided symmetry transformations strictly and update the policy accordingly. The main purpose of these loss functions is to find

a symmetric outcome, independently of perturbations in the reward function, the agent (control process), the robot or the environment. As an example, consider a humanoid robot with a rusty left arm. The limb still has the same range of motion as the right one, but the amount of torque required to produce the same outcome is different. Assuming that for a given task, no motor needs to reach its maximum torque, there is a symmetry transformation that maps the torque difference between both arms to achieve the equivalent outcome in the symmetric state. For this example, the proposed algorithm finds a function that rectifies biases and achieves a symmetric outcome.

Nevertheless, a symmetric outcome is not always desirable, either due to biases introduced by the environment in favor of asymmetric behaviors, or due to explicit problem constraints expressed through the reward function. To generalize the algorithm to these cases, its purpose can be redefined as adapting symmetric transformation(s) in order to maximize the return. In general terms, this can be achieved by finding functions that best describe the relation between sets of two action dimensions across all states and symmetric transformations.

An ASL overview is shown in Fig.2. Initially, in addition to defining hyperparameters for the actor-critic method (PPO) and the symmetry algorithm, the user has to provide the same information required by previous symmetry loss functions — the best known estimate for every symmetry transformation. Each transformation must include a vector of functions to transform states and actions. Symmetry transformations can be omitted if the user deems them to be unrelated or detrimental to the problem being optimized, but this is not required.

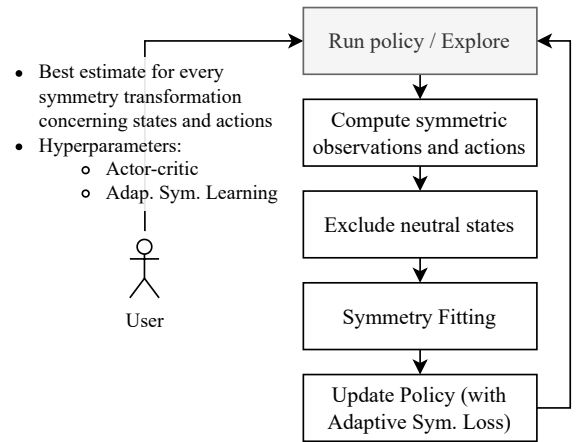


Fig. 2. Adaptive Symmetry Learning algorithm overview

The algorithm starts by running the current policy and exploring the action space to gather a batch of samples (states, actions, rewards). Symmetric observations and actions are computed and stored, and neutral states are excluded based on a user-defined threshold (see Section IX-B for details on the exclusion method). Then, the provided symmetry transformations suffer a small adjustment in direction of the policy and, finally, the policy is updated. The final loss used to compute the gradient that updates the policy is a sum of PPO's loss and the Adaptive Symmetry Loss. So, in this last step, the policy suffers a small adjustment in direction of the symmetry

transformation.

Consequently, there is a circular relation between reinforcement learning and symmetry fitting. However, the former learns the behavior (the best action for each state), while the latter learns constant state-independent perturbations from several sources, as enumerated in the beginning of this section. An alternative perspective is to consider the symmetry fitting as a moving average of the symmetric transformations learned by the policy (where the most recent average sample is restricted to the last batch of explored states). A more detailed explanation is given in the following sections.

VIII. ADAPTIVE SYMMETRY LEARNING: SYMMETRY FITTING

An overview of the symmetry fitting process is shown in Fig. 3. Before learning, the algorithm extracts and groups types of mappings between action dimensions (from the provided symmetry transformations). Using humans as an example, with respect to the sagittal plane, each two distinct body parts that mirror each other form symmetric *pairs*, while central body parts like the head form reflexive relations (*singles*). Circular symmetry relations of 3 or more body parts (*cycles*) do not exist in humans. Nonetheless, models with *cycles* have additional restrictions as will be discussed in Section VIII-A4.

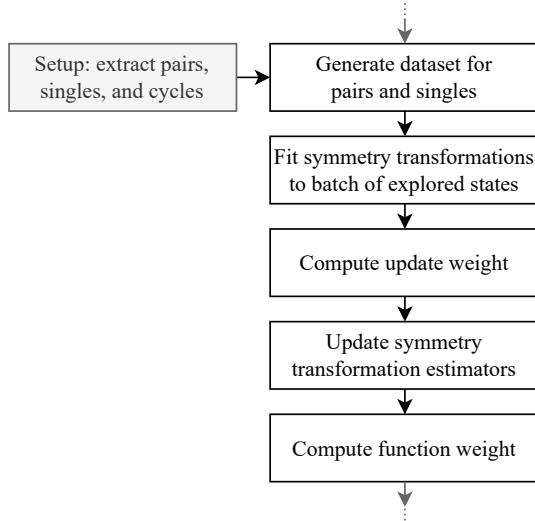


Fig. 3. Overview of the symmetry fitting process

The process is executed after the exploration phase, when local symmetry transformations are fitted to the policy. The term *local* indicates that only the last batch of states from the exploration phase is used to generate the dataset. Local transformations are used as target for the global transformation estimators, according to an update weight. This weight is based on cycle restrictions, if they exist, otherwise a fixed weight is used, as defined by the user. Finally, the targets used to update each function in the transformation vectors are assessed in terms of stability to compute a function weight employed by the symmetry loss to penalize unstable functions. These topics will be reviewed in detail, in the following paragraphs, through an example robot model.

Inspired by a triangular lamina example by McWeeny [34], consider a 2D robot shaped as an equilateral triangle with 3 controllable limbs that are able to rotate around axes located at each vertex of the robot (see Fig. 4, top left). For the symmetry of a figure to be absolutely known, all its non-equivalent symmetry properties must be determined [35]. Assuming the robot cannot be flipped, it has 6 non-equivalent symmetry operations characterized by 3 symmetry planes (**a**, **b**, **c**) and 3-fold rotational symmetry (**d**, **e**), i.e., it is invariant under rotations of 120, 240 or 360 deg, although the last one is an identity operation. Therefore, in total, only 5 symmetry operations are to be considered (see Fig. 4, top middle).

Rotating 240 deg is equivalent to performing two 120 deg rotations. This means that, although both operations must be declared, in theory, only the specification of 120 deg should be needed. Yet, currently, ASL does not allow the specification of combined symmetry operations, which means that 5 specifications are required. Despite this limitation, the algorithm will automatically simplify redundant operations, as explained in the end of the next section.

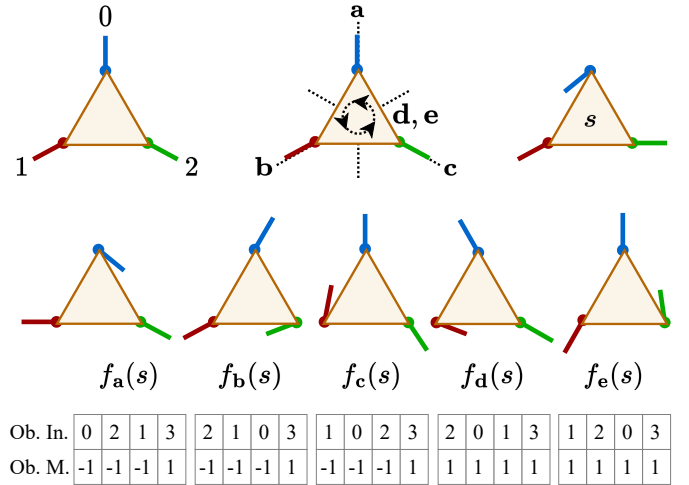


Fig. 4. 2D robot shaped as an equilateral triangle with 3 limbs, 3 symmetry planes (**a**, **b**, **c**) and 3-fold rotational symmetry (**d**, **e**). $f_a(s)$, $f_b(s)$, $f_c(s)$, $f_d(s)$ and $f_e(s)$ are symmetry transformations of s relative to **a**, **b**, **c**, **d** and **e**, respectively. The observations indices and multipliers characterize the transformations above.

A. Setup

The state space of the robot is represented by 4 observed variables $[X_0, X_1, X_2, Z]$, where X_i is the angular position of limb i relative to its neutral position (let the positive rotation direction be counterclockwise), and Z is the battery level. The purpose of Z is to introduce a variable that is not affected by symmetry transformations. In the top right corner of Fig. 4 is represented an arbitrary state s , and in the bottom are represented the states that result from applying the 5 aforementioned symmetric transformations (e.g. $f_a(s)$ is the reflection of s in relation to symmetry plane **a**).

Below $f_a(s)$ to $f_e(s)$ are two rows of values that characterize the respective transformation. The top row specifies how to rearrange the variables of s (observation indices) and the

bottom row indicates if an inversion is necessary (observation multipliers). Transformation f_a , for instance, is a vector of functions such that

$$f_a(s) = [f_a[0](s[0]), f_a[1](s[2]), f_a[2](s[1]), f_a[3](s[3])]. \quad (25)$$

Given the observation multipliers in Fig. 4, it is possible to simplify the equation to

$$f_a(s) = [-s[0], -s[2], -s[1], s[3]]. \quad (26)$$

The new value for X_0 is given by $X_0 \cdot -1$ (same limb but inverted rotation direction), but limb 1 gets the inverted value of limb 2 and vice versa. Since the battery level is not affected by this transformation, $X_3 \leftarrow X_3 \cdot 1$. As observed, the rotation direction was inverted for every limb, and the same is true for $f_b(s)$ and $f_c(s)$, but not for $f_d(s)$ and $f_e(s)$, which require no inversion.

The robot has 3 action variables $[Y_0, Y_1, Y_2]$, where Y_i is the torque applied to limb i . In this case, given action a , the symmetry transformations $g_a(a)$, $g_b(a)$, $g_c(a)$, $g_d(a)$ and $g_e(a)$ are analogous to the already introduced transformations, excluding the battery level (see the respective actions indices and multipliers in Fig. 5).

	$g_a(a)$	$g_b(a)$	$g_c(a)$	$g_d(a)$	$g_e(a)$
Act. In.	$\begin{bmatrix} 0 & 2 & 1 \\ 0 & 2 & 1 \end{bmatrix}$	$\begin{bmatrix} 2 & 1 & 0 \\ 2 & 1 & 0 \end{bmatrix}$	$\begin{bmatrix} 1 & 0 & 2 \\ 1 & 0 & 2 \end{bmatrix}$	$\begin{bmatrix} 2 & 0 & 1 \\ 2 & 0 & 1 \end{bmatrix}$	$\begin{bmatrix} 1 & 2 & 0 \\ 1 & 2 & 0 \end{bmatrix}$
Act. M.	$\begin{bmatrix} -1 & -1 & -1 \\ -1 & -1 & -1 \end{bmatrix}$	$\begin{bmatrix} -1 & -1 & -1 \\ -1 & -1 & -1 \end{bmatrix}$	$\begin{bmatrix} -1 & -1 & -1 \\ -1 & -1 & -1 \end{bmatrix}$	$\begin{bmatrix} 1 & 1 & 1 \\ 1 & 1 & 1 \end{bmatrix}$	$\begin{bmatrix} 1 & 1 & 1 \\ 1 & 1 & 1 \end{bmatrix}$

Fig. 5. Action indices and multipliers that characterize the 2D robot's symmetry transformations $g_a(a)$, $g_b(a)$, $g_c(a)$, $g_d(a)$ and $g_e(a)$

As mentioned in the beginning of Section IX, in some circumstances, it is possible to achieve a symmetric outcome with perturbations in the control process, the robot or the environment. Therefore, it is possible to leverage the same symmetric principles if the motors of the 2D robot behave differently due to several factors (e.g. different power specifications, unbalanced control drivers, or external factors such as rust). As a basic example, consider that limb 1 is rusty and requires double the normal torque to perform the same movement, and limb 2 requires triple the normal torque. Until either motor reaches its maximum torque, the symmetric transformations can be described as in Fig. 6.

	$g_a(a)$	$g_b(a)$	$g_c(a)$	$g_d(a)$	$g_e(a)$
Act. In.	$\begin{bmatrix} 0 & 2 & 1 \\ 0 & 2 & 1 \end{bmatrix}$	$\begin{bmatrix} 2 & 1 & 0 \\ 2 & 1 & 0 \end{bmatrix}$	$\begin{bmatrix} 1 & 0 & 2 \\ 1 & 0 & 2 \end{bmatrix}$	$\begin{bmatrix} 2 & 0 & 1 \\ 2 & 0 & 1 \end{bmatrix}$	$\begin{bmatrix} 1 & 2 & 0 \\ 1 & 2 & 0 \end{bmatrix}$
Act. M.	$\begin{bmatrix} -1 & -\frac{2}{3} & -\frac{3}{2} \\ -1 & -\frac{2}{3} & -\frac{3}{2} \end{bmatrix}$	$\begin{bmatrix} \frac{1}{3} & -1 & -3 \\ \frac{1}{3} & -1 & -3 \end{bmatrix}$	$\begin{bmatrix} -\frac{1}{2} & -2 & -1 \\ -\frac{1}{2} & -2 & -1 \end{bmatrix}$	$\begin{bmatrix} \frac{1}{3} & 2 & \frac{3}{2} \\ \frac{1}{3} & 2 & \frac{3}{2} \end{bmatrix}$	$\begin{bmatrix} \frac{1}{2} & \frac{2}{3} & 3 \\ \frac{1}{2} & \frac{2}{3} & 3 \end{bmatrix}$

Fig. 6. Hypothetical action indices and multipliers in a scenario where limb 1 is rusty and requires double the normal torque and limb 2 requires triple the normal torque. This transformation holds while both affected motors are below saturation.

In some situations the symmetric transformations that lead to the highest return may not be known a priori. In Fig. 6, the transformation operation can be defined as a linear equation

of the form $y = mx$, where x is an arbitrary action and m is the action multiplier vector. On the one hand, different problems may require more complex functions to describe the required operation. On the other hand, the policy (typically parameterized by a neural network) is already able to represent complex non-linear relations. So, if a linear function can approximate the symmetric relation to a satisfactory degree, it should be preferred, as complex functions have increased learning time, potentially counteracting the sample efficiency benefit of using symmetries.

During its initialization, the symmetry fitting process extracts pairs of symmetric action dimensions from the user-defined action indices. In the current scenario, there are 3 pairs $\{(0,1), (0,2), (1,2)\}$, which means that the 15-dimensional operation represented in Fig. 5 and Fig. 6 can be reduced to a 3-dimensional problem. The relations between each pair of action dimensions can be written in the form $a'[y] = m_{x \rightarrow y} \cdot a[x]$. Fig. 7 shows how the action multipliers in Fig. 6 could be reduced to functions of the three proportional relations between pairs $m_{0 \rightarrow 1}$, $m_{0 \rightarrow 2}$ and $m_{1 \rightarrow 2}$.

	$g_a(a)$	$g_b(a)$	$g_c(a)$	$g_d(a)$	$g_e(a)$
Act. In.	$\begin{bmatrix} 0 & 2 & 1 \\ 0 & 2 & 1 \end{bmatrix}$	$\begin{bmatrix} 2 & 1 & 0 \\ 2 & 1 & 0 \end{bmatrix}$	$\begin{bmatrix} 1 & 0 & 2 \\ 1 & 0 & 2 \end{bmatrix}$	$\begin{bmatrix} 2 & 0 & 1 \\ 2 & 0 & 1 \end{bmatrix}$	$\begin{bmatrix} 1 & 2 & 0 \\ 1 & 2 & 0 \end{bmatrix}$
Act. M.	$\begin{bmatrix} -1 & -\frac{1}{m_{0 \rightarrow 2}} & -\frac{1}{m_{0 \rightarrow 1}} \\ -1 & -\frac{1}{m_{0 \rightarrow 2}} & -\frac{1}{m_{0 \rightarrow 1}} \end{bmatrix}$	$\begin{bmatrix} -\frac{1}{m_{0 \rightarrow 2}} & -1 & -\frac{1}{m_{0 \rightarrow 1}} \\ -\frac{1}{m_{0 \rightarrow 2}} & -1 & -\frac{1}{m_{0 \rightarrow 1}} \end{bmatrix}$	$\begin{bmatrix} -\frac{1}{m_{0 \rightarrow 1}} & -\frac{1}{m_{0 \rightarrow 2}} & -1 \\ -\frac{1}{m_{0 \rightarrow 1}} & -\frac{1}{m_{0 \rightarrow 2}} & -1 \end{bmatrix}$	$\begin{bmatrix} \frac{1}{m_{0 \rightarrow 1}} & \frac{1}{m_{0 \rightarrow 2}} & 1 \\ \frac{1}{m_{0 \rightarrow 1}} & \frac{1}{m_{0 \rightarrow 2}} & 1 \end{bmatrix}$	$\begin{bmatrix} \frac{1}{m_{0 \rightarrow 2}} & \frac{1}{m_{0 \rightarrow 1}} & m_{0 \rightarrow 2} \\ \frac{1}{m_{0 \rightarrow 2}} & \frac{1}{m_{0 \rightarrow 1}} & m_{0 \rightarrow 2} \end{bmatrix}$
			IV II	I	III

Fig. 7. Rewriting the action multipliers from Fig. 6 as a function of three pair relations of the form $a'[y] = m_{x \rightarrow y} \cdot a[x]$. Highlighted in red are action multipliers that depend on $m_{0 \rightarrow 1}$.

1) *Generate dataset for pairs:* After running the policy and collecting a batch of explored states, the symmetry fitting procedure can be executed. The first step is to generate a dataset to fit the user-defined function. This step is repeated for every pair of action dimensions, but for the sake of conciseness, only pair (0,1) will be analyzed. The objective is to fit a function $F : \mathbb{R} \rightarrow \mathbb{R}$, such that $a'_t[1] = F(a_t[0])$ for $t \in \{0, 1, \dots, B\}$, where B is the batch size. The direction of such relation is $0 \rightarrow 1$ because it transforms the action associated with limb 0 to that of limb 1.

The dataset does not depend on actions sampled during exploration. Instead, in line with previously introduced symmetry loss functions, it uses the distribution mean to reduce noise. It is limited to states that were explored because the process of fitting symmetric transformations relies on what the policy has learned. Including rare or unreachable states would be counterproductive since the policy could produce unreliable results.

The dataset is generated as seen in Table I, with one column for input values and another one for output values. There are four variations of the same relation in symmetry transformations $g_c(a)$, $g_d(a)$ and $g_e(a)$. Relation (I) in $g_d(a)$ (see Fig. 7) follows the desired direction $0 \rightarrow 1$ (because under

$g_{\mathbf{a}}(a)$, $m_{0 \rightarrow 1}$ is the value we multiply by $a[0]$ to obtain $a'[1]$. So, the inputs are directly obtained from the distribution mean for every state s_t in the latest batch ($\bar{a}_0[0]$), and the outputs are obtained from the distribution mean for all $f_{\mathbf{d}}(s_t)$ ($\bar{a}'_{\mathbf{d},t}[1]$).

TABLE I
EXTRACTION OF DATASET FROM POLICY TO LEARN THE SYMMETRIC TRANSFORMATION FOR THE ACTION PAIR (0,1)

Local relation	Input (x)	Output (y)
0 \rightarrow 1 (I)	$\bar{a}_0[0]$	$\bar{a}'_{\mathbf{d},0}[1]$

0 \rightarrow 1, reflection (II)	$\bar{a}_B[0]$	$\bar{a}'_{\mathbf{d},B}[1]$
	$-\bar{a}_0[0]$	$\bar{a}'_{\mathbf{c},0}[1]$
1 \rightarrow 0 (III)	$\bar{a}'_{\mathbf{e},0}[0]$	$\bar{a}_0[1]$

1 \rightarrow 0, reflection (IV)	$\bar{a}'_{\mathbf{e},B}[0]$	$\bar{a}_B[1]$
	$-\bar{a}'_{\mathbf{c},0}[0]$	$\bar{a}_0[1]$

	$-\bar{a}'_{\mathbf{c},B}[0]$	$\bar{a}_B[1]$

For relation (II), symmetry plane \mathbf{c} requires limb 1 to mirror limb 0 (inverting the rotation direction), yielding $a'_t[1] = G(a_t[0])$. Function $G : \mathbb{R} \rightarrow \mathbb{R}$ expresses the local relation, which is a reflection of F about the vertical axis, such that $G(a_t[0]) = F(-a_t[0])$. To fix this discrepancy, the sign of inputs for the second local relation in Table I is reversed.

Relation (III) is similar to relation (I) except that the direction is $1 \rightarrow 0$ and thus, the inputs and outputs are swapped. Finally, relation (IV) requires an inversion of inputs and outputs and a sign reversal for the inputs due to the local reflection.

2) *Generate dataset for singles*: Symmetry transformations $g_{\mathbf{a}}(a)$, $g_{\mathbf{b}}(a)$ and $g_{\mathbf{c}}(a)$ also contain reflexive relations (singles), i.e., relations from and to the same action dimension. In Fig. 7, singles have an action multiplier of -1 , which means that in the symmetric state, the symmetric action consists in rotating the same limb but in the opposite direction. One limitation of reflexive relations is that they must be characterized by involutory functions to avoid the complexity of state dependency. This notion is better understood with a practical example.

Fig. 8 denotes a practical use case for symmetry fitting, where limb 0 of the previously introduced 2D robot is subjected to a constant force pointing to the weight. Note that the weight is just a representation of the perturbation, which can have multiple sources, including the environment or robot defects.

On the left side of Fig. 8 is represented state s . Assume that limb 0 has a relatively short range of motion and the perturbation manifests as a constant torque of $+3$ being applied to limb 0 (positive torque means clockwise direction). Let $a[0] = -8$ be the optimal action in s for limb 0 and $a[0] = 2$ the optimal action in the symmetric state $f_{\mathbf{a}}(s)$. Function $g_{\mathbf{a}}[0](a) = -a[0] - 6$ is a linear approximation of the symmetric transformation for the corresponding action dimension. This function is symmetric across the line $y = x$ and, consequently, involutory. This means that for any symmetry plane and any state $g_{\mathbf{a}}(g_{\mathbf{a}}(a))[0] = a[0]$.

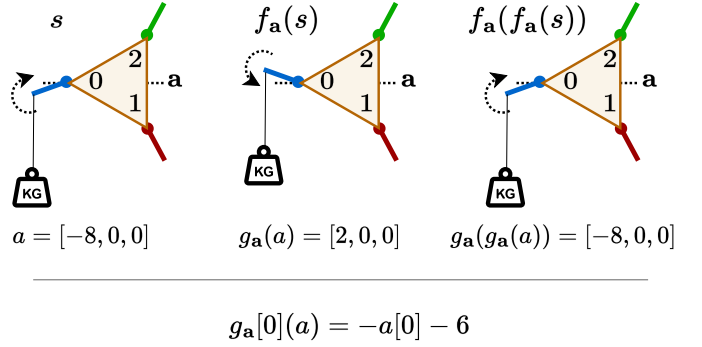


Fig. 8. Practical use case for symmetry fitting, where the symmetric action transformation can be approximated by a linear involutory function, that does not depend on the environment state

A linear functions of the form $y = mx + b$ is involutory if $m = -1$ or $m = 1 \wedge b = 0$. Fig. 9 presents another practical use case for symmetry fitting, where the symmetric action transformation depends on the position of limb 0 ($s[0]$). The diagonal grid in Fig. 9 is a high friction area relative to the robot's body, where limb 0 must apply twice as much torque to overcome the extra friction. Therefore, when the limb is below symmetry plane \mathbf{a} , or more formally, the angular position of limb 0 is positive ($s[0] > 0$), the symmetric transformation is given by $g_{\mathbf{a}}[0](a) = -2a[0]$. The rotation direction is inverted and the torque is multiplied by 2 to counteract the friction and obtain a symmetric outcome. However, when $s[0] < 0$, the inverse function is needed $g_{\mathbf{a}}[0](a) = -0.5a[0]$.

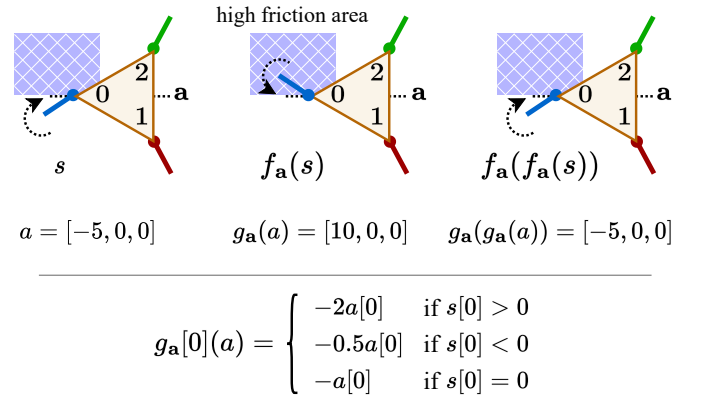


Fig. 9. Practical use case for symmetry fitting, where the symmetric action transformation is dependent on the environment state because it is not characterized by an involutory function

Since $y = -2x$ is not involutory, a 3D piecewise function is required, as defined in the bottom of Fig. 9. Recall that g is a function of state-action pairs (s, a) , even though the implicit state s is omitted, as mentioned in Section II-A. Considering a problem where the ground truth is unknown (e.g. a high friction area of unknown location or shape), fitting a symmetry transformation would require the algorithm to learn the number of sub-functions, the parameters of each sub-function and the associated subdomains. The possible ramifications of this problem are outside the scope of this paper.

Therefore, to avoid the complexity of state dependency, symmetry transformations for singles are limited to involutions. The dataset for singles is a simplified version of Table I since reflexive relations have a unique direction (e.g. $0 \rightarrow 0$). Moreover, linear transformations are a special case that reduces the number of local relations to one. As aforementioned, involutory linear functions of the form $y = mx + b$ are constrained by $m = 1 \wedge b = 0$ or $m = -1$. The former constraint has no learnable parameter, so it is not included in the dataset. The latter defines a negative relation and can be included in the dataset to learn parameter b . Since there are no positive learnable relations, there is no need to perform reflections about the vertical axis (reversing the sign of inputs), thus reducing the effective number of local relations to one.

3) *Optimization*: A possible solution for this problem is to use the method of least squares to fit an arbitrary function F parameterized by ν to the dataset

$$\arg \min_{\nu} \sum_{i=1}^U (y_i - F_{\nu}(x_i))^2, \quad (27)$$

where U is the number of inputs and outputs extracted from the policy. If F is a linear function, the method formulation can be reduced to ordinary least squares, to which there is a constant-time analytical solution

$$m, b = \arg \min_{m, b} \sum_{i=1}^U (y_i - mx_i - b)^2, \quad (28)$$

$$m = \frac{U(\sum_i x_i y_i) - (\sum_i x_i)(\sum_i y_i)}{U(\sum_i x_i^2) - (\sum_i x_i)^2}, \quad (29)$$

$$b = \frac{(\sum_i y_i) - m(\sum_i x_i)}{U}. \quad (30)$$

For singles, only parameter b can be learned in linear functions, simplifying the solution

$$\begin{aligned} b &= \arg \min_b \sum_{i=1}^U (y_i + x_i - b)^2 \\ &= \frac{(\sum_i x_i) + (\sum_i y_i)}{U}. \end{aligned} \quad (31)$$

For pairs, having a bias component b can be useful in certain scenarios, as will be discussed in Section XIII. However, for the sake of completeness, fixing b reduces (28) to

$$\begin{aligned} m &= \arg \min_m \sum_{i=1}^U (y_i - mx_i)^2 \\ &= \frac{(\sum_i x_i y_i)}{(\sum_i x_i^2)}. \end{aligned} \quad (32)$$

4) *Cycles*: The described optimization problem can have additional restrictions if there are circular relations of 3 or more pairs (hereinafter referred to as cycles). In the 2D robot example, the pairs of symmetric action dimensions $\{(0,1),(0,2),(1,2)\}$ form a single cycle (0 to 1 to 2), although it can also be represented as (2 to 1 to 0) since all relation pairs are bidirectional. One important property of cycles is that the composition of all functions in a cycle is an identity

transformation $\text{id} : \mathbb{R} \rightarrow \mathbb{R}$, such that $\text{id}(x) = x$, e.g., $F_{0 \rightarrow 1} \circ F_{1 \rightarrow 2} \circ F_{2 \rightarrow 0} = \text{id}$. Plugging this equality constraint into (27), and generalizing to an example with P pairs and C cycles yields

$$\arg \min_{\nu} \sum_{j=1}^P \sum_{i=1}^{U_j} (y_i - F_{\nu_j}(x_i))^2, \quad (33)$$

$$\text{subject to } (F_{\nu_{T_0^0}} \circ F_{\nu_{T_1^0}} \circ F_{\nu_{T_2^0}} [\circ \dots])(1) = 1,$$

...

$$(F_{\nu_{T_0^C}} \circ F_{\nu_{T_1^C}} \circ F_{\nu_{T_2^C}} [\circ \dots])(1) = 1,$$

where T_a^b is a jagged array indicating the a -th pair index of cycle b , e.g. $T_0^1 = 2$ means that the first (0) pair associated with cycle 1 is the overall second (2) pair (0,2), for which F_{ν_2} is the corresponding transformation function. Using cycle-based constraints increases the optimization complexity due to the constraint incorporation and the fact that pair relations contained in cycles can no longer be computed independently of each other. Moreover, there are typically numerous local minima that obey the constraints, making the optimization more sensitive to small differences in the dataset. In practice, during training, this technique introduced a substantial amount of variance in the estimation of F_{ν} .

An alternative approach is to optimize each transformation independently using (27), and then compute an update weight based on the cycle error ϵ . For pair (q, u) , the update weight $w_{U(q,u)}$ can be computed through a user-defined function $H_U : \mathbb{R}_0^+ \rightarrow [0, 1]$, such that

$$w_{U(q,u)} = \min(H_U(\epsilon_0), \dots, H_U(\epsilon_C)), \quad (34)$$

$$\text{with } \epsilon_i = \left| (F_{\nu_{T_0^i}} \circ F_{\nu_{T_1^i}} \circ F_{\nu_{T_2^i}} [\circ \dots])(1) - 1 \right|,$$

where C is the number of cycles that includes pair (q, u) . An example for function H_U is $H_U(x) = 0.05 \times 0.01 / (0.01 + x^4)$, where 0.05 is the maximum update weight, and $0.01 / (0.01 + x^4)$ is a decaying factor dependent on the cycle error.

5) *Transformation Update*: During the optimization stage, the algorithm finds the best parameter vector ν for each function, considering only the last batch of explored states. To reduce variance, the optimized parameter vector is seen as a target for an exponential moving average. Assuming relations of the form $y = mx + b$, there are two targets (T_m, T_b) per pair, yielding the update rules for the estimated parameters

$$\hat{m} \leftarrow \hat{m} + w_U * (T_m - \hat{m}), \quad (35)$$

$$\hat{b} \leftarrow \hat{b} + w_U * (T_b - \hat{b}). \quad (36)$$

As seen earlier, each symmetric transformation function corresponds to a specific pair of symmetric action dimensions. For the 2D robot example, there are 3 pairs, and each function is associated with multiple symmetry planes or rotations (see Fig. 7). Note that updating $m_{0 \rightarrow 1}$, $m_{0 \rightarrow 2}$ and $m_{1 \rightarrow 2}$ directly influences 12 action multipliers. In Fig. 7, $b_{0 \rightarrow 1}$, $b_{0 \rightarrow 2}$ and

$b_{1 \rightarrow 2}$ are assumed to be initially zero, but these values can also be learned, influencing 12 action biases. Analogously, learning reflexive relations ($b_{0 \rightarrow 0}$, $b_{1 \rightarrow 1}$ and $b_{2 \rightarrow 2}$) directly influences the remaining 3 action biases.

6) *Function weight*: For the 2D robot example, there are 5 symmetric action transformations, each representing a vector of 3 functions (1 per limb). At an early optimization stage, the policy is mostly random and, consequently, the symmetry fitting targets tend to have high standard deviation σ . As the convergence starts, σ is progressively reduced, albeit at different rates for distinct functions. Furthermore, a constant high σ (in successive batches of explored states) may indicate that a given function is not a good estimator for the symmetric transformation. For these reasons, when targets have high σ , the respective function estimator has less importance in the symmetry loss.

For a given estimator function parameterized by vector \mathbf{x} , let μ_{x_i} and σ_{x_i} be the mean and standard deviation of the target value for parameter x_i , respectively, in the last k_1 iterations, where k_1 is a hyperparameter. The metric used to assess the recent target spread is the absolute value of the coefficient of variation, based on the definition of Everitt and Skrondal [36], $c_v = \sigma/|\mu|$. This metric is important to reduce the relative standard deviation as the mean increases. However, to avoid instability near $\mu = 0$, a small constant (0.1) is added to the function weight w_F equation

$$w_F = \text{H}_F\left(\frac{\sigma}{|\mu| + 0.1}\right), \quad (37)$$

where $\text{H}_F : \mathbb{R}_0^+ \rightarrow [0, 1]$ is a user-defined function that transforms the spread metric into a weight between 0 and 1. The function weight w_F will be used later by the symmetry loss in (57).

IX. ADAPTIVE SYMMETRY LEARNING: LOSS FUNCTION

The Adaptive Symmetry Learning loss function computes a novel loss that tackles problems such as neutral states or dis-advantageous updates. Additionally, symmetry transformation estimators are used according to their reliability, as defined above by w_F . The algorithm is characterized by the following equation:

$$L^{ASL}(\theta, \omega) = \hat{\mathbb{E}}_t [w_\pi \cdot L_t^\pi(\theta) + w_V \cdot L_t^V(\omega)], \quad (38)$$

$$\text{with } L^\pi(\theta) = -\hat{\mathbb{E}}_t [r_t(\theta) \cdot \psi_t \cdot \phi_t], \quad (39)$$

$$L^V(\omega) = \hat{\mathbb{E}}_t [(V_\omega(f(s_t)) - V_t^{\text{targ}})^2 \cdot \psi_t \cdot \phi_t], \quad (40)$$

where L^π and L^V are the policy and value losses for symmetry, and w^π and w^V are the respective weight factors. The value loss reduces the difference between the value function (for the symmetric state), and the same value target used by PPO. The policy loss promotes a policy symmetrization with a restricted update. This behavior is partly achieved through a dead zone gate ψ and a value gate ϕ , both based on user-defined thresholds. The former rejects neutral states or those

that are near neutrality (see Section IX-B), and the latter avoids changing the symmetric action if it is more valuable than the current action (see Section IX-C).

However, the main progression restriction is imposed by the ratio r_t , which works similarly to PPO's ratio (9), except that the restriction is applied on the target action τ_t instead of the ratio itself, and the policy's standard deviation σ is not actively modified:

$$r_t(\theta) = \frac{\pi_\theta(\tau_t, f(s_t) \mid \mu_\theta, \sigma)}{\pi_{\theta_{\text{old}}}(\tau_t, f(s_t) \mid \mu_{\theta_{\text{old}}}, \sigma)}, \quad (41)$$

$$\tau_t = \text{clip}(g(\mu_{\theta_{\text{last}}}(s_t)), \bar{a}'_t - \Delta\mu, \bar{a}'_t + \Delta\mu), \quad (42)$$

where \hat{A}_t is PPO's advantage function estimator; a_t is the action sampled at time t ; \bar{a}_t (5) and \bar{a}'_t (6) are the mean of the distribution when a_t was sampled for states s_t and $f(s_t)$, respectively; $g(\mu_{\theta_{\text{last}}}(s_t))$ is the mean of the distribution after the last mini-batch update; and $\Delta\mu$ is a user-defined restriction threshold explained in the following subsection.

The mean $g(\mu_{\theta_{\text{last}}}(s_t))$ represents the most recent action for state s_t . It is similar to $g(\mu_{\theta_{\text{old}}}(s_t))$ in the sense that it is a non-trainable constant, but it is updated during the optimization stage, at every mini-batch update of every train epoch. In (42), $g(\mu_{\theta_{\text{last}}}(s_t))$ could be replaced by the explored action a_t in the cases where a_t has a positive advantage estimate ($\hat{A}_t \geq 0$), since PPO would try to increase a_t 's relative probability. However, doing that would subvert PPO's trust region by allowing the symmetry update to exploit the sampled action in a greedy way. Moreover, the objective of the symmetry update is not to explore, but rather to motivate symmetry in a nondestructive way.

As an example, consider a bidirectional variable-speed conveyor belt that is trying to center an item, and the state indicates whether the item is on the left or the right side. Assume that initially the neural network outputs a speed of -5 for both cases, leading every item to eventually fall to the left. After some exploration, the policy finds that for an item on the right, a speed of $a_t \sim \pi_\theta(s_t) = -2$ is advantageous (as it increases the time the item spends near the center). Let $\Delta\mu = 0.5$. The target τ_t becomes $\text{clip}(5, -5 - 0.5, -5 + 0.5) = -4.5$. Ideally, after every mini-batch update, $\mu_{\theta_{\text{last}}}(s_t)$ gets closer to -2, leading to a target of $\text{clip}(2, -5 - 0.5, -5 + 0.5) = -4.5$. In this scenario the target does not change because the action for the symmetric state is too far from $g(\mu_{\theta_{\text{last}}}(s_t))$. Large symmetry updates could harm the policy by changing the neural network too much.

If the target is exceeded (e.g. $\mu_\theta(f(s_t)) = -4.4$), the gradient of $r_t(\theta)$ will try to move the policy back to the target. In an analogous situation, PPO would only stop motivating further progress towards its sampled target. This harsh symmetry restriction has the purpose of breaking momentum build-ups, as explained in the next subsection. Now assume that after hours of training, the NN outputs -10 and 10 for an item on the right and left sides, respectively. Yet, it finds that 11 is advantageous for the left side item. The target τ_t becomes $\text{clip}(-10, -10 - 0.5, -10 + 0.5) = -10$, which produces no difference. However, as $\mu_\theta(s_t)$ increases to 10.1 along several

mini-batch updates, the target decreases to $\tau_t = -10.1$. So, the symmetric action closely follows the sampled action until it reaches -10.5. If the symmetric limitation is small enough, PPO’s loss function will dominate the update direction, allowing for asymmetric updates, if required.

The next subsection delves into the motivation and design of the restricted update, and one of its most critical parameters — the distribution’s mean shift $\Delta\mu$. It also provides context for the standard deviation preservation in (41), and the momentum build up issues. The following subsections derive the dead zone and value gates, ψ and ϕ from (39); present a condensed implementation of the loss function and summarize all ASL’s hyperparameters.

A. Restricted update

Both PPO and TRPO [37] apply the trust region concept as depicted in Fig. 1. During policy updates, the target relative probability of a certain action is restricted by a soft limit imposed by the clipping parameter ϵ . As an example, consider an explored action with a positive estimated advantage ($\hat{A}_t > 0$), and $\epsilon = 0.3$. The loss function gradient will motivate a relative probability growth of 30%, although the new relative probability can surpass that soft limit due to the influence of other actions in the update batch, or the optimizers used to update network weights.

As the policy follows a normal distribution, there are 2 parameters that can influence the relative probability for a given action: the mean μ_θ and the standard deviation σ . The mean is parameterized by a neural network and altering it means shifting the preferred action for a given state, while the standard deviation expands or narrows the exploration around said action. For symmetry, there are three key differences in relation to the original concept of trust region:

- 1) For a given time step t there is always exactly one desired action, so the objective is to always increase the relative probability of its symmetric counterpart (except to enforce the trust region as explained in point 3);
- 2) Since the update direction is known a priori, there is no need for exploration, so it could be risky for the symmetry loss to modify the policy’s standard deviation σ , as it could negatively affect the main algorithm. The Proximal Symmetry Loss’s term $\pi_{\theta_{old}}(a_t | s_t)$ in (21) attempts to mitigate this issue by limiting the relative probability of the symmetric action. However, ideally, the symmetry loss should not actively modify σ ;
- 3) While using common momentum-based optimizers such as Adaptive Moment Estimation (Adam) [38], the trust region applied to constant targets is inherently hard to control, as the constant update direction can build up momentum and easily override asymmetric exploration. There are at least three ways of overcoming this issue: not using momentum-based optimizers, which comes at a heavy cost; reduce the symmetry weight so that the noise created by the total loss is enough to prevent cyclic patterns (as applied by the PSL); or create a fixed target at the trust region border, which actively reduces the relative probability of the symmetric action

if it exceeds the region, instead of simply not motivating further progress, as does PPO. This last solution is used by ASL in (41) and (42).

It is important to control the influence of symmetry in exploration and harmonize the final loss function. To understand the best approach, we need to analyze the average PPO update for a single time step, considering the above mentioned restrictions. Fig. 10 shows the relation between exploration and target policy update for a single time step. Action $a = \mu_{\theta_i} + k_e\sigma$ has a positive estimated advantage and follows a univariate normal distribution with fixed standard deviation. Exploration parameter k_e defines the distance of the sampled action to the initial mean of the distribution μ_{θ_i} in relation to σ . The gradient of PPO’s loss function motivates the initial relative probability p_i of action a_t to increase until $p_i \cdot \epsilon$. Assuming an ideal update, the neural network shifts the distribution’s mean to μ_{θ_f} . The relation between k_e and the distribution mean shift $\Delta\mu$ will allow us to replicate that behavior for the symmetry update.

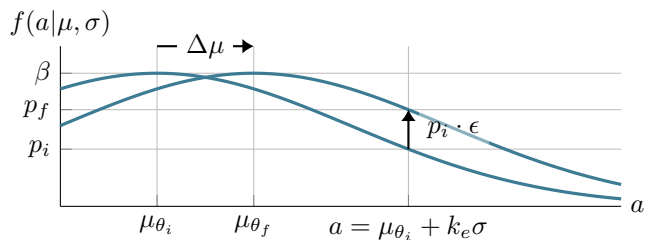


Fig. 10. Relation between: (1) distance of an advantageous explored action (a_t) to the distribution mean before the update (μ_{θ_i}) and (2) the progress of the distribution. Assume an ideal update with the trust region and a policy that follows a univariate normal distribution with fixed standard deviation.

However, this example deals with univariate distributions, and typical reinforcement learning environments have high-dimensional actions spaces. In PPO, the clipping parameter ϵ limits the relative probability of the action as a whole. Considering the notion of joint probability for independent events, each dimension has an average soft limit

$$\xi = \sqrt[n]{1 + \epsilon} - 1, \quad (43)$$

where n is the number of dimensions. Although the PPO loss function does not require this dimension-level specification, the explored action uses an independent standard deviation value for each dimension, so it makes sense to also establish individual targets for each dimension.

The following derivation considers the relation between k_e and $\Delta\mu$ for a single dimension. Let the probability density function (PDF) for a univariate normal distribution be $f(x|\mu, \sigma) = \beta e^{-\frac{1}{2}(\frac{x-\mu}{\sigma})^2}$, with $\beta = 1/(\sigma\sqrt{2\pi})$. The distribution mean shift $\Delta\mu$ can be obtained as the distance from a_t to the largest a for which the PDF of $\mathcal{N}(\mu_{\theta_i}, \sigma)$ is p_f :

$$p_i = f(\mu_{\theta_i} + \epsilon\sigma | \mu_{\theta_i}, \sigma) = \beta e^{-\frac{1}{2}k_e^2}, \quad (44)$$

$$p_f = \min((1 + \xi)p_i, \beta), \quad (45)$$

$$\begin{aligned} \Delta\mu &= \mu_{\theta_i} + k_e\sigma - f^{-1}(p_f | \mu_{\theta_i}, \sigma) \\ &= \mu_{\theta_i} + k_e\sigma - \mu_{\theta_i} - \sigma \sqrt{-2 \cdot \ln \frac{\min((1 + \xi)\beta e^{-\frac{1}{2}k_e^2}, \beta)}{\beta}} \\ &= \sigma \left(k_e - \sqrt{-2 \cdot \ln \min((1 + \xi)e^{-\frac{1}{2}k_e^2}, 1)} \right), \quad (46) \end{aligned}$$

where $f^{-1}(x|\mu, \sigma) = \mu + \sigma\sqrt{-2\ln(x/\beta)}$ is the largest solution for the inverse PDF. Fig. 11 shows the plot of $\Delta\mu$ as a function of k_e , for a typical clipping value $\epsilon = 0.2$ [39] and 3 action space dimensions $n \in \{4, 16, 64\}$. For each function represented in Fig. 11, the maximum at $k_e = \sqrt{-2\ln(1/(1 + \xi))}$, separates the linear part on the left, from the non-linear part on the right (that corresponds to Fig. 10). The linear case happens when $\mu_{\theta_f} = a_t$.

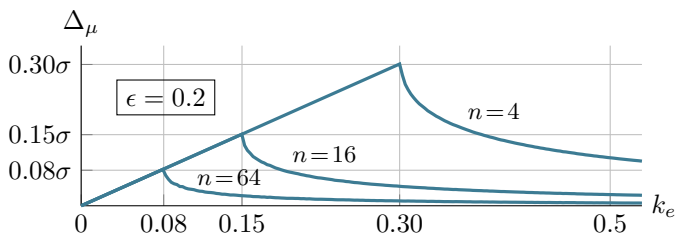


Fig. 11. Plot of the distribution's mean shift $\Delta\mu$ as a function of k_e with $\xi = \sqrt[3]{1 + 0.2} - 1$ and $n \in \{4, 16, 64\}$

Empirically, restricting the symmetry update such that $\Delta\mu \geq \sigma\sqrt{-2\ln(1/(1 + \xi))}$ serves no purpose, other than to accelerate the symmetry convergence at the beginning of training. Therefore, for the sake of simplicity, the update restriction can be reduced to

$$\Delta\mu = k_s\sigma\sqrt{-2\ln\frac{1}{1 + \xi}}. \quad (47)$$

In both cases, the restriction is given in relation to σ and ξ . However, instead of defining the distance of the artificially explored symmetric action through k_e , and then compute the maximum distribution shift, we are defining that shift directly through k_s . Consequently, the stationary point from Fig. 11 is removed and $\Delta\mu(k_s|\sigma, \xi)$ becomes a linear function, as shown in Fig. 12.

The unit value for k_e and k_s also has a different meaning. Choosing $k_e = 1$ means adopting PPO's update behavior for an action sampled at 1 standard deviation from the distribution's mean ($a = \mu_{\theta_i} \pm \sigma$), assuming a constant σ . Alternatively, defining $k_s = 1$ means adopting PPO's update behavior for the action that would yield the largest update, also assuming a constant σ . Moreover, defining $k_s > 1$ has an intuitive meaning, since the update magnitude increases monotonically.

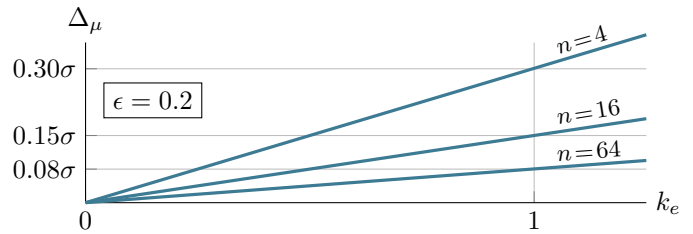


Fig. 12. Plot of the distribution's mean shift $\Delta\mu$ as a function of k_s with $\xi = \sqrt[3]{1 + 0.2} - 1$ and $n \in \{4, 16, 64\}$

B. Exclusion of neutral states

As introduced in Section II-D, neutral states and neighboring areas in the state space pose a significant challenge for learning efficient behaviors through symmetric policies. ASL provides the option to reject regions that surround neutral states through a dead zone gate ψ_t :

$$\psi_t = \begin{cases} 1, & \text{if } \frac{1}{n} \sum_{i=1}^n (\delta_{t,i}) > k_d, \\ 0, & \text{otherwise} \end{cases}, \quad (48)$$

$$\text{with } \delta_{t,i} = \frac{|s_{t,i} - f(s_{t,i})|}{\text{MAD}_i}, \quad (49)$$

$$\text{and } \text{MAD}_i = \frac{\sum_{t=1}^{k_t} |s_{t,i} - \bar{s}_i|}{k_t}, \quad (50)$$

where MAD_i is the mean absolute deviation of state s for state dimension i , for the last k_t time steps (typically $k_t = 10 \cdot B$, where B is the batch size). Parameter $\delta_{t,i}$ represents the relative distance between state s and its symmetric counterpart $f(s)$, for a specific time step t and state dimension i .

The dead zone gate ψ_t is 0 if s_t is relatively close to a neutral state, and 1 otherwise. When $\psi_t = 0$ in (39) and (40), the gradients of L^{ASL} w.r.t. θ and ω ignore time step t . In practice, the policy is free to learn asymmetric behaviors near neutral states, thus circumventing the problem stated in Section II-D.

C. Value gate

Analogously to PSL's unidirectional update (see Section VI-A), ratio r_t in (41) promotes an adjustment to $\pi_\theta(f(s_t))$ without changing $\pi_\theta(s_t)$. As already concluded, adapting the symmetric action is better than the explored action because the explored action is more likely to be optimal than the symmetric action.

This approach can be improved by comparing the estimated value of the explored and symmetric actions, and then blocking updates when the symmetric action is considerably more valuable. To achieve that purpose, a value gate ϕ_t yields 1 to allow an update, or 0 to block it, based on a user defined parameter $k_v \in (1, +\infty)$, such that

$$\phi_t = \begin{cases} 1, & \text{if } v_t > V_\omega(f(s_t)) \\ 0, & \text{otherwise} \end{cases}, \quad (51)$$

$$\text{with } v_t = \begin{cases} k_v \cdot V_\omega(s_t), & \text{if } V_\omega(s_t) \geq 0 \\ \frac{V_\omega(s_t)}{k_v}, & \text{otherwise} \end{cases}. \quad (52)$$

Although setting $k_v = 1$ would obviate the need for (52), simplifying the condition in (51) to $V_\omega(s_t) > V_\omega(f(s_t))$, it revealed to be counterproductive in early tests, since many time steps were being blocked due to inaccuracies in the value function estimator. Therefore, to reduce the gate sensitivity, it is recommended to use values for k_v well above 1 (e.g. 1.5). Since k_v is a proportional factor, it is required to distinguish when $V_\omega(s_t)$ is positive and negative, as illustrated in Fig. 13.

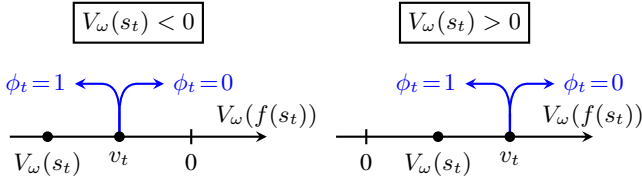


Fig. 13. Value gate ϕ_t behavior when the explored state value $V_\omega(f(s_t))$ is negative (left) and positive (right). The difference lies in how the auxiliary variable v_t is obtained.

In both cases, the update is blocked ($\phi_t = 0$) when the value of the symmetric state is larger than v_t , being the only difference the way v_t is calculated. Using a proportional factor v_t instead of adding a constant is important to deal with outlier states with unusually small or large values.

D. Implementation

This subsection presents a condensed implementation of ASL's loss function, compiling the final form of all previously explained modules. Rewriting (38) as an empirical average over a finite batch of B samples for N symmetries yields:

$$L^{ASL}(\theta, \omega) = \sum_{j=1}^N \frac{1}{B} \sum_{t=1}^B [w_j^\pi \cdot L_{j,t}^\pi(\theta) + w_j^V \cdot L_{j,t}^V(\omega)], \quad (53)$$

$$\text{with } L_{j,t}^\pi(\theta) = -r_{j,t}(\theta) \cdot \psi_{j,t} \cdot \phi_{j,t}, \quad (54)$$

$$L_{j,t}^V(\omega) = (V_\omega(f_j(s_t)) - V_t^{\text{targ}})^2 \cdot \psi_{j,t} \cdot \phi_{j,t}. \quad (55)$$

The ratio $r_{j,t}$ between two probability densities can be simplified, considering that both deal with the same standard deviation variable σ , and by applying the quotient rule for exponents with the same base:

$$\begin{aligned} r_{j,t}(\theta) &= \frac{\pi_\theta(\tau_{j,t}, f_j(s_t) \mid \mu_\theta, \sigma)}{\pi_{\theta_{\text{old}}}(\tau_{j,t}, f_j(s_t) \mid \mu_{\theta_{\text{old}}}, \sigma)} \\ &= \frac{\frac{1}{(2\pi)^{n/2} \prod_i \sigma_i} \cdot \exp\left(-\frac{1}{2} \sum_{i=1}^n \frac{(\tau_{j,t,i} - \mu_{\theta_i}(f_j(s_t)))^2}{\sigma_i^2}\right)}{\frac{1}{(2\pi)^{n/2} \prod_i \sigma_i} \cdot \exp\left(-\frac{1}{2} \sum_{i=1}^n \frac{(\tau_{j,t,i} - \bar{a}'_{j,t,i}(f_j(s_t)))^2}{\sigma_i^2}\right)} \\ &= \exp\left(\sum_{i=1}^n \frac{(\tau_{j,t,i} - \bar{a}'_{j,t,i})^2 - (\tau_{j,t,i} - \mu_{\theta_i}(f_j(s_t)))^2}{2 \cdot \sigma_i^2}\right), \end{aligned} \quad (56)$$

where $\bar{a}'_{j,t} = \mu_{\theta_{\text{old}}}(f_j(s_t))$ and n is the number of dimensions of each action. Plugging in the function weight w_F defined in (37) for symmetry fitting:

$$r_{j,t}(\theta) = \exp\left(\sum_{i=1}^n \frac{(\tau_{j,t,i} - \bar{a}'_{j,t,i})^2 - (\tau_{j,t,i} - \mu_{\theta_i}(f_j(s_t)))^2}{2 \cdot \sigma_i^2 / w_{j,i}^F}\right) \quad (57)$$

Target τ_t , distribution mean shift $\Delta\mu$ and dead zone gate ψ_t can be rewritten for a specific symmetry index j with minimum changes:

$$\tau_{j,t} = \text{clip}(g_j(\mu_{\theta_{\text{last}}}(s_t)), \bar{a}'_{j,t} - \Delta\mu_j, \bar{a}'_{j,t} + \Delta\mu_j), \quad (58)$$

$$\Delta\mu_j = k_j^s \sigma \sqrt{-2 \ln \frac{1}{1 + \xi}}, \quad (59)$$

$$\psi_{j,t} = \begin{cases} 1, & \text{if } \frac{1}{n} \sum_{i=1}^n (\delta_{j,t,i}) > k_j^d \\ 0, & \text{otherwise} \end{cases}, \quad (60)$$

$$\text{with } \delta_{j,t,i} = \frac{|s_{t,i} - f_j(s_{t,i})|}{\text{MAD}_i}, \quad (61)$$

$$\text{and } \text{MAD}_i = \frac{\sum_{t=1}^{k_t} |s_{t,i} - \bar{s}_i|}{k_t}, \quad (62)$$

where ξ is defined in (43). Value gate ϕ_t can also be easily adapted to a specific symmetry index j but the auxiliary variable v_t can be improved for parallel computation by replacing the branch with an equivalent equation:

$$\phi_{j,t} = \begin{cases} 1, & \text{if } v_t > V_\omega(f_j(s_t)) \\ 0, & \text{otherwise} \end{cases}, \quad (63)$$

$$\text{with } v_t = \alpha \cdot V_\omega(s_t) + (k_v - \alpha) |V_\omega(s_t)|, \quad (64)$$

where α is an auxiliary constant equal to $(k_v^2 + 1)/(2k_v)$.

E. Hyperparameters

The hyperparameters described in previous subsections are summarized in Table II. Most parameters are vectors with one scalar per symmetry operation. The exceptions are system-wide parameters that include $\mathbf{g}(a)$ form, H_U , H_F and k_t .

TABLE II
ASL HYPERPARAMETERS

Symbol	Description	Section
$f(s)$	symmetric state transformation	II-A
$g(a)$	symmetric action transformation	II-A
w_π	policy symmetry loss weight	VII
w_v	value symmetry loss weight	VII
$g(a)$ form	function form of $g(a)$	VIII
H_U	cycle penalty function	VIII-A4
H_F	action transformation penalty function	VIII-A6
k_s	maximum distribution shift	IX-A
k_d	dead zone around neutral state	IX-B
k_t	time steps for neutral state rejection	IX-B
k_v	value gate proportional factor	IX-C

X. EVALUATION ENVIRONMENT

The experiments for this paper were executed in PyBullet — a physics simulator based on the Bullet Physics SDK [40]. An ant robot based on the AntBulletEnv-v0 environment was chosen as the base to develop several learning scenarios. This robot model was selected due to the type and number of symmetry transformations under which it is invariant.

The ant robot, shown in Fig. 14, is a four-legged robot with 8 joints and actuators. Joint 0 controls the rotation of one leg around the robot’s z-axis, and joint 1 controls the knee rotation for the same leg. The remaining joints control the other legs in an equivalent way. The robot has 4 planes of symmetry: xy-plane, yz-plane, $y=x$ and $y=-x$. Additionally, it has 4-fold rotational symmetry around the z-axis. More specifically, the robot is invariant under rotations of 90, 180, 270 or 360 deg around the z-axis, although the last rotation is an identity operation.

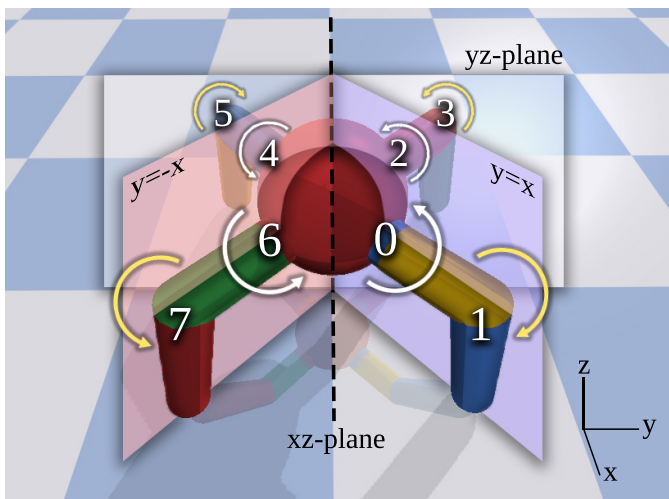


Fig. 14. AntBulletEnv-v0’s robot has 8 joints/actuators. Even joints rotate around the robot’s z-axis, and odd joints (ant’s knees) rotate around a vector orthogonal to the z-axis. The arrows show the positive rotation direction for each joint. The robot has 4 planes of symmetry, xy-plane, yz-plane, $y=x$ and $y=-x$, and 4-fold rotational symmetry around the z-axis.

The state space for all ant-based scenarios is listed in Table III. The first observation indicates the relative height of the robot in comparison to the height at the beginning of an episode, which is fixed. The second observation is a unit vector

parallel to the ground that indicates the goal direction, relative to the robot. After the relative linear velocity of the robot, roll and pitch, comes the vector $[p_0, s_0, p_1, s_1, \dots, p_7, s_7]$, where p_x and s_x are the position and speed of joint x . Finally, a binary value indicates whether each foot is touching the ground.

TABLE III
ANTBULLETV0’S STATE SPACE

Index	Description
0	height - initial height
1-2	unit goal vector (y,x)
3-5	linear velocity (x,y,z)
6-7	roll (x), pitch (y)
8-23	position/speed of joints 0-7
24-27	feet contact (boolean)

The symmetry transformations are determined as explained in Section VIII-A. Consider the xz-plane depicted in Fig. 14. The respective action transformation is composed of 8 *action indices* and 8 *action multipliers*, as listed in the top two rows of Fig. 15. Note that a positive action in all dimensions will cause knee flexion at joints 1 and 7, and knee extension at joints 3 and 5. Although for the xz-plane this results in direct proportion, for the yz-plane the relation is inverted.

xz-plane	action indices								obs. indices																			
	action multipliers								obs. multipliers																			
0	1	2	3	4	5	6	7	20	21	22	23	16	17	18	19	12	13	14	15	8	9	10	11	27	26	25	24	
1	-1	1	1	-1	-1	-1	-1	1	1	1	-1	-1	-1	1	1	-1	-1	1	1	-1	-1	1	1	1	1	1	1	1

Fig. 15. xz-plane symmetry transformation for AntBulletEnv-v0

The last two rows in Fig. 15, correspond to the *observation indices* and *observation multipliers*). The first column corresponds to the robot height as presented in Table III. The height is invariant to any of the symmetry planes or rotations, so its index corresponds to itself, and the multiplier is 1. For the unit goal vector (y, x) , y must be inverted and x is invariant. Therefore, the index is kept unchanged (1 and 2), and the multiplier is -1 and 1, respectively. This logic can be applied to all the elements of Table III to fill the remaining columns of *observation indices* and *observation multipliers*. See Appendix A for the symmetry transformations concerning the remaining symmetry transformations.

XI. EVALUATION SCENARIOS

In all scenarios, the main objective is to go in the direction of the goal. The original reward function from AntBulletEnv-v0 was not changed, and it encompasses: stay-alive bonus, progress towards the objective, electricity cost, joints-at-limit cost to discourage stuck joints, and foot collision cost. An episode ends if the ant’s torso makes contact with the ground or after 1000 steps.

A. Main objective

Contrary to training a single goal direction like the original AntBulletEnv-v0, the proposed scenarios define 8 possible directions with a fixed angular distance of 45 deg as shown in

Fig. 16. For a batch of episodes, the goal generation is sequential (0 to 7) and not random, in order to reduce the variability while training and also to reduce biases when periodically evaluating the policy. In our environment implementation (see Section XII-A), to minimize code modifications, we changed the initial robot orientation instead of the goal location.

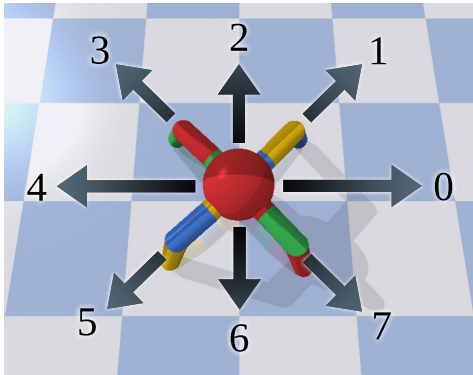


Fig. 16. Sequence of goals for 8-directional ant locomotion

During preliminary experiments the robot had a tendency to move towards the goal with one front leg, one back leg, and 2 side legs. In practice, if the goals were 1, 3, 5 or 7, the robot would move without rotating its body, while for other goals, it would first rotate until one of the legs was pointing to the goal. To prevent this bias, in addition to the terminal conditions applied by the original AntBulletEnv-v0 environment, the episode is terminated if the robot’s orientation deviates more than 25 deg from its initial value. Fig. 17 presents sequential frames of example runs where the robot is pursuing goal 6 (bottom) and 7 (top).

B. Controlled scenarios

The first set of proposed scenarios is listed in Table IV. Scenario **A1.1** assumes that no perturbation is introduced by the robot, environment, reward function or control mechanism. The action modifier vector from the second column is multiplied by the policy’s output (a vector of ones means no modification). The third column indicates the range to which the action is clipped after being modified. For Scenario **A1.1**, all action dimensions are clipped to $[-1,1]$ before being sent to the robot. The last column indicates the goals used during training, where the index corresponds to the goal numbering denoted in Fig. 16. During evaluation, all scenarios presented in Table IV are tested for goals 0 to 7.

TABLE IV
EVALUATION SCENARIOS I

Scenario	Action Mod. (AM)	Action Range	Train goals
A1.1	[1,1,1,1,1,1,1,1]	-1 to 1	0-7
A1.2	[1,1,1,1,1,1,1,1]	-1 to 1	0,1
A2.1	[0.65,0.75,...,1.35]	-1 to 1	0-7
A2.2		-AM to AM	
A3.1	[0.30,0.50,...,1.70]	-1 to 1	0-7
A3.2		-AM to AM	

Scenario **A1.2** is similar in all aspects, except the training goals. While training, the robot is only exposed to goals 0

and 1 but, during evaluation, it is still tested on all goals (0-7). In theory, according to the ant robot’s symmetry planes and rotations, symmetry-aware algorithms should be able to transpose the knowledge from goal 0 to (2, 4, 6) and from goal 1 to (3, 5, 7).

The remaining scenarios from Table IV simulate an artificial perturbation in the action controller. In **A2**, each action dimension is multiplied by a value in the vector $[0.65,0.75,...,1.35]$. **A2.1** then clips the values between -1 and 1. In this case all motors are equivalent, there is only a control imbalance. This means that a symmetric outcome is still possible if the perturbation is compensated by the policy.

However, **A2.2** clips the action values between $[-0.65,-0.75,...,-1.35]$ and $[0.65,0.75,...,1.35]$. Now, some actuators have different maximum torque values (e.g. the maximum torque for the knee at joint 1 in relation to the knee at joint 7 is 55%). This problem is not trivial and requires asymmetric learning, independently of perturbation corrections. In this example, the ability to perform symmetric actions in symmetric states is not guaranteed. Scenarios **A3** are a harder version of **A2** in terms of action modification.

C. Realistic scenarios

A second set of scenarios listed in Table V was devised to test realistic robot and environment perturbations. As mentioned in the beginning of Section XI, AntBulletEnv-v0’s reward function has a stay-alive bonus. Its purpose is to reward the agent for lifting its torso above the ground at all times. Yet, in harsh conditions, the agent may learn to exploit the stay-alive bonus by not moving, since any wrong movement can end the episode earlier. To avoid changing the reward function, a new condition was added to the environment for the second set of scenarios — the episode ends if no progress was made towards the goal in the last 30 steps.

TABLE V
EVALUATION SCENARIOS II

Scenario	Feet Mass	Surface	Train Goals	Eval. Goals
A4.1	[40,20, κ , κ]	flat	0-7	
A4.2			1,3,5,7	
A4.3			0,2,4,6	
A5.1	0,1,2,3		0-7	
A4.4	0-7			
A4.5	1,3,5,7			
A4.6	[40, κ ,20, κ]	0,2,4,6		
A5.2	0,1,2,3		0-7	
A6.1	[κ , κ , κ , κ]	5° tilt Dir: 0	0-7	
A6.2			1,3,5,7	
A6.3			0,2,4,6	
A6.4		5° tilt Dir: 1	0-7	
A6.5			1,3,5,7	
A6.6			0,2,4,6	

In Table V, the second column specifies the mass of each foot, where the first vector element corresponds to the foot connected to joint 1 (see Fig. 14), followed by joints 3, 5 and 7. The default mass κ is 13.5. Scenarios **A4.1** to **A4.3** modify the mass of the first and second feet. **A4.1** is trained and evaluated on all goals. **A4.2** handles only odd goals (1,3,5,7) while **A4.3** handles only even goals (0,2,4,6). Scenarios **A4.4** to **A4.6** work

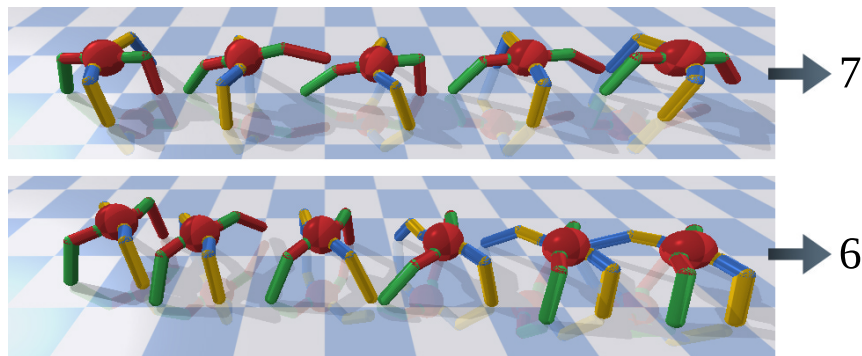


Fig. 17. Sequential frames of the ant robot moving to the right, in pursuit of goal 6 (bottom) and 7 (top)

in a similar way, except that they modify the first and third feet.

An explanation is required for some of the design choices. First, the different mass configurations are an attempt to create a large amount of perturbation patterns across all symmetry planes and rotations. Second, the modified mass values (40, 20) are a trade-off between disrupting existing models (i.e. models trained without the modification have no control over the robot after the modifications) and allowing training (since joint actuators have limited torque). Third, the train and evaluation goals are separated into groups to allow the additional assessment of 2 types of locomotion (associated with the odd and even goals).

Scenarios **A5.1** and **A5.2** are a complement to the perturbations tested in **A4.1** and **A4.4**, respectively, but the agent is only able to train on half of the goals. The objective is for the algorithm to learn the perturbations with the training goals and generalize that knowledge to the remaining goals. In this experiment, allowing only two training goals, like in **A1.2**, would make the symmetry fitting unfeasible, since some symmetric states would never be experienced — hence the 4 training goals.

Finally, scenarios **A6** follow a similar setup to **A4** but instead of modifying the feet mass, the surface is tilted 5 deg. For **A6.1** to **A6.3**, the tilt is in direction of goal 0 (i.e. gravity pulls the robot towards goal 0), and for **A6.4** to **A6.6**, the tilt is in direction of goal 1. It is important to note that if the agent was able to know the tilt direction through observations, there would be no need for symmetry fitting. If for instance, the roll and pitch observations (see Table III) were relative to the ground and not the tilted surface, the agent would know the tilt direction. Consider the example presented as follows.

Fig. 18 on the left, shows a scenario where the platform is tilted in direction of goal 6. In each episode, the ant would chase a different goal direction, but the green and blue feet would always be stepping on higher ground, when directly compared to the other two feet (note that the robot cannot rotate more than 25 deg or the episode is terminated). So, for instance, considering the xz -plane, the symmetric state (on the right) is unreachable, and the algorithm will not leverage symmetry for this symmetry plane. This is the case for all symmetry rotations and symmetry planes, except for the yz -plane because it is aligned with the tilt direction. In conclusion,

this is not a scenario where a symmetry loss function would be very useful.

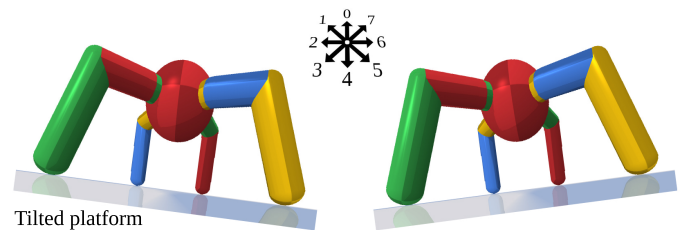


Fig. 18. Experienced tilted state (left) and its symmetric state in relation to the xz -plane (right)

With this in mind, it is possible to make use of symmetric states and symmetry loss functions when the perturbation is not part of the state space (i.e. it is not observable). In this way, the optimization algorithm will be able to generalize, to a certain extent, the learned behavior to the symmetric states, even if in practice the initial symmetry transformations do not accurately represent reality.

To make sure the roll and pitch observations were not affected, instead of tilting the surface, we changed the gravity vector to achieve the equivalent effect.

XII. EVALUATION METHODOLOGY

The performance in each scenario was evaluated for four algorithms: PPO (without any extension), PPO+ASL (PPO extended with Adaptive Symmetry Learning), PPO+PSL (PPO extended with Proximal Symmetry Loss), and PPO+MSL (PPO extended with Mirror Symmetry Loss). MSL and PSL employ the improved versions introduced in Section V and VI, respectively.

All experiments were conducted on a single machine with two Intel Xeon 6258R with 28 cores. In total, 908 distinct hand-tuned configurations were tested. Each configuration was used to train 12 models. Typically, between 48 and 96 models were learned in parallel, requiring between 12h and 24h. A new set of hand-tuned configurations was designed after each learning round.

Automatic tuning approaches were not used for two main reasons. First, the ASL algorithm was tweaked during the experiments to fix errors and test new methods and implementation techniques. This process requires constant human

intervention since auto-tuning methods do not detect problems in the algorithm. Second, due to time and computational constraints, hand-tuning was the only viable option in terms of efficiency.

A. Codebase

The implementation of each extension was made in Python on top of a Stable Baselines 3 repository fork [41]. This codebase was chosen due to its high quality implementation, considering how specific code-optimizations can have a deep impact on PPO’s performance [42]. The final code allows the user to select any of the aforementioned extensions per symmetry transformation, allowing for versatile combinations of symmetry extensions and parameters, although in the scope of this work, symmetry extensions were evaluated independently to allow for a fair comparison. All the algorithm implementations tested in this work, as well as code modification to the ant environment are available at our GitHub repository².

B. Hyperparameters

The choice of hyperparameters for PPO is crucial to enable successful applications, and should be tuned case by case [43]. However, for consistency among scenarios and algorithms, a fixed set of hyperparameters was used, as listed in Table VI.

TABLE VI
PPO HYPERPARAMETERS

Parameter	Value	Parameter	Value
batch steps	4096	mini-batch size	64
clip range	0.4	NN activation	ReLU
entropy coefficient	0	NN log std init	-1
environments	1	NN orthogonal init	false
epochs	20	normalize advantage	true
GAE λ (lambda)	0.9	policy NN	[256,256]
γ (gamma)	0.99	value coefficient	0.5
learning rate	3×10^{-5}	value NN	[256,256]
max. gradient norm	0.5		

The chosen values were adapted from the RL Baselines3 Zoo training framework [44]. The number of environments was reduced from 16 to 1 to improve performance while training parallel models (by eliminating the thread synchronization overhead). Considering this modification and the increased complexity imposed by the proposed scenarios, in comparison with the original AntBulletEnv-v0 environment, some other parameter values were changed: batch steps, mini-batch size and the total time steps (which is defined per scenario).

Regarding the evaluated symmetry algorithms, their hyperparameters were tuned per scenario. Nonetheless, the values presented in Table VII were common to all cases. Symmetry transformations $f(s)$ and $g(a)$ represent the initial knowledge about the ant robot, assuming a perturbation-free system. The remaining hyperparameter vectors in Table VII were assigned a scalar as a slight abuse of notation to convey that the same scalar was assigned to all symmetry transformations, with the exception of $k_d[\text{rot}]$, which concerns only the subset of rotations.

²<https://github.com/m-abr/Adaptive-Symmetry-Learning>

TABLE VII
COMMON ASL HYPERPARAMETERS

Method	Symbol	Short Description	Value
all	$f(s)$	sym. state transf.	Fig. 15 and 20
all	$g(a)$	sym. action transf.	
all	w_v	value sym. loss weight	0.5
ASL	H_U	cycle penalty	$0.05 \cdot \frac{10^{-2}}{(10^{-2}+x^4)}$
ASL	H_F	action transf. penalty	1.1^{-x}
ASL	$k_d[\text{rot}]$	dead zone (rotation)	0
ASL	k_t	time steps (neutral state)	$10 \times (\text{batch steps})$
ASL	k_v	value gate factor	1.5

The value symmetry loss function is the same in all evaluated symmetry algorithms. Since $w_v^{PPO} = w_v^{ASL} = w_v^{PSL} = w_v^{MSL}$ typically produces good results, and $w_v^{PPO} = 0.5$ (see Table VI), parameter w_v was also set to 0.5 for all symmetry algorithms.

In the scenarios tested in this paper, neutral states affect reflections but not rotations. Every time a rotation transformation is applied, the unit goal vector from the state space (see Table III) is also rotated, so the symmetric state can never be the same as the initial state, which is a necessary condition for neutral states. For that reason $k_d = 0$ for all rotations. For reflections, k_d was set independently for each scenario. The remaining parameters from Table VII were found to be consistent across all experiments.

C. Metrics

All algorithms were evaluated and compared in terms of performance. Additional metrics were used to analyze symmetric properties. The reinforcement learning process alternates between training for 15 iterations (15×4096 batch steps), and evaluating the policy for 16 episodes (using the deterministic neural network output), as depicted in Fig. 19. Some variables are logged every 5 iterations, depending on the chosen symmetry extension, and are an average over the last 4096 time steps. For all metrics, each data point is then averaged again for 12 independent instances. In total, four variables were generated:

- 1) Average episode return — the undiscounted return provides a raw measure of performance that takes into consideration all the implicit objectives defined in the reward function;
- 2) Average value distance — absolute difference between the value estimates of the explored state and the corresponding symmetric state. This metric assesses how accurately the current symmetry transformations describe the policy for explored states;
- 3) Average neutral state rejection ratio (NSRR) — ratio of states that were rejected by the Adaptive Symmetry Learning algorithm (see Section IX-B). The NSRR measures to what extent the neutral state rejection module was actually applied to each symmetry plane: xz-plane, yz-plane, y=x plane, and y=-x plane.
- 4) Average symmetry transformation targets — target values for the current action transformation approximation to a user-defined parameterized function. For linear

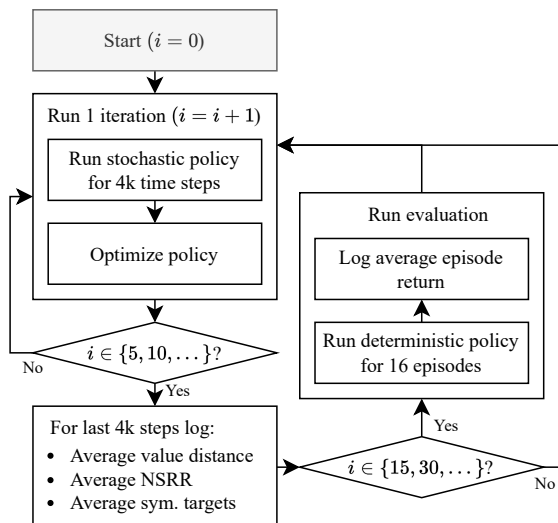


Fig. 19. Reinforcement learning flowchart with integrated performance evaluation every 15 iterations. Some variables are logged every 5 iterations.

functions, the ant model has 12 action multipliers (e.g. $m_{0 \rightarrow 2}$) and 16 actions biases (12 based on symmetric pairs, such as $b_{0 \rightarrow 2}$, and 4 based on reflexive relations such as $b_{0 \rightarrow 0}$ or b_0). This metric evaluates the repeatability of results while comparing independent optimizations, and the accuracy of the learned action transformations if the ground truth is known. A detailed explanation for linear approximations is given in the next paragraph.

The problem of learning action transformations (see their initial values in Fig. 15 and 20) can be simplified due to the existence of redundant symmetry relations. The ant model has 8 actions and 7 non-identity symmetry transformations, totaling 56 action transformations. Consequently, there are 112 variables if the operations can be defined as linear equations of the form $a'[y] = m_{x \rightarrow y} \cdot a[x] + b_{x \rightarrow y}$, or 56 variables if b is not considered. Analogously to the process described in Fig. 7, the ant's action transformations can be written as a function of 12 pairs of symmetric action dimensions $\{(0,2),(0,4),(0,6),(1,3),(1,5),(1,7),(2,4),(2,6),(3,5),(3,7),(4,6),(5,7)\}$ and 4 singles $\{0,2,4,6\}$, yielding 12 actions multipliers and 16 biases (28 variables for $y = mx + b$ operations).

XIII. EVALUATION RESULTS

The hyperparameters used for each scenario are listed in Appendix B and the evaluated metrics are plotted in Appendix C. Below are discussed the results for each scenario. For the purpose of this analysis, PPO without any extension is considered the baseline.

Due to lacking a mandatory progression condition, the controlled scenarios (A1.1 to A3.2) exhibit a similar behavior in the beginning of training (see Fig. 21). The local peak at approximately 3×10^5 time steps corresponds to the algorithm learning how to exploit the stay-alive bonus by not moving to avoid irrecoverable mistakes, as explained in Section XI-C.

Then, the slight drop coincides with a more exploratory phase, where the agent starts taking risks.

The average symmetry transformation target error in Fig. 24 was only plotted for scenarios A2 and A3. For A2.1 and A3.1 the ground truth is known. Let x be the action multiplier vector shown in the second column of Table IV. Consider for instance the symmetric relation between two action dimensions a_0 and a_2 . To achieve a symmetric outcome, the equality $a_0 x_0 = a_2 x_2$ must hold. Therefore, the transformation parameterized by $m_{0 \rightarrow 2}$ can be obtained such that

$$\begin{cases} a_0 x_0 = a_2 x_2 \\ a_2 = a_0 m_{0 \rightarrow 2} \end{cases} \Rightarrow a_0 x_0 = a_0 m_{0 \rightarrow 2} x_2 \Rightarrow m_{0 \rightarrow 2} = \frac{x_0}{x_2}. \quad (65)$$

So, in Fig. 24, the ground truth for $[m_{0 \rightarrow 2}, m_{0 \rightarrow 4}, \dots, m_{5 \rightarrow 7}]$ is given by $[0.76, 0.62, 0.52, 0.79, 0.65, 0.56, 0.81, 0.68, 0.83, 0.70, 0.84, 0.85]$ for A2.1, and $[0.43, 0.27, 0.20, 0.56, 0.38, 0.29, 0.64, 0.47, 0.69, 0.53, 0.73, 0.76]$ for A3.1. Since the ground truth for A2.2 and A3.2 is unknown, for comparison, we reuse the values used for A2.1 and A3.1, respectively.

The remaining of this section delves into the discussion of specific results for each scenario. For the sake of simplicity, when mentioning ASL, it should be read as PPO+ASL, and the same is true for the other symmetry extensions.

A1.1

All symmetric algorithms performed similarly in this scenario, contrasting with the baseline, as depicted in Fig. 21 for 4 million time steps. ASL performed best without symmetry fitting, which indicates that linear modifications to the symmetry transformations yield no advantage in this context. In terms of average value distance (see Fig. 22), all the symmetry extensions follow a common pattern of allowing asymmetric exploration until around 2.2×10^6 time steps, before the model starts to converge to the provided symmetric transformations.

The average NSRR for ASL shown in Fig. 23 reveals the contrast between both gaits depicted in Fig. 17 in terms of neutral state incidence. When walking with one front leg, a symmetric policy is a good policy if and only if the initial position is perfectly aligned with the objective, and there is no perturbation in the policy or environment. These conditions are impractical, even more so due to the initial random component introduced by AntBulletEnv-v0. Nonetheless, walking with one front leg results in an increasing number of neutral states as the policy converges to local optima, resulting in an increasing NSRR for planes $y=x$ and $y=-x$. In contrast, walking with two front legs rarely generates neutral states, hence the low NSRR for planes xz and yz .

A1.2

In comparison with the previous scenario, the policy was only able to train on goals 0 and 1, having to generalize its behavior to the other 6 goals. In this setting, ASL outperformed the other three methods, and itself in A1.1. Both symmetry fitting and the value gate were disabled. Since most value estimates were being modified by the value loss and not by exploration, the value gate lost its purpose and became

counterproductive, consequently being disabled. Therefore, the only modules that contributed to this performance were the ratio with fixed standard deviation in (56), and neutral state rejection (Section IX-B).

The value distance plots show that the policies under all symmetry methods converged earlier to the symmetric transformations, which led to a steeper learning curve in all three cases. The NSRR of planes yz and $y=-x$ was zero during training because the agents only trained on goals 0 and 1. Yet, the NSRR for plane $y=x$ indicates that convergence to the symmetric transformations was much faster in comparison with **A1.1**, and for the xz -plane it was constantly higher. These results show that symmetry in gaits is correlated with performance in this scenario, and that generalizing to symmetric states can be more efficient when training only in a subset of non-symmetrically-redundant states. Note that in **A1.1**, the policy is also being generalized to symmetric states. The only difference is that states similar to those generalized also occur during training in **A1.1**.

A2

From this point forward, symmetry fitting was enabled on all experiments. In **A2.1**, the introduced modifiers are proportional to the action, and in **A2.2** there is an additional non-linear component. In both cases, as supported by the value distance plots, the ASL policies are following the learned symmetry transformation closer, in comparison with the other methods. In **A2.1**, the learning curve is identical to **A1.1**, indicating that symmetry fitting was able to compensate the action modifiers without performance loss, while PSL and MSL experienced some decay by having the extra effort of learning an asymmetric policy. In **A2.2**, as expected, symmetry fitting could only handle linear perturbations, resulting in less advantage over the other approaches. This difference is also evident from the NSRR data, when comparing both scenarios with **A1.1**.

By observing Fig. 24, it is possible to conclude that the learned symmetry transformations are very similar in both **A2.1** and **A2.2**, and the respective error relative to the ground truth of **A2.1** converges to the vicinity of zero. Note that the initial symmetry transformation had an average error of 0.282 and, after training, that value dropped to 0.031 on **A2.1** and 0.049 on **A2.2**.

A3

Due to the difficulty of this and following scenarios, the training was prolonged to 5 million time steps. **A3.1** and **A3.2** are harder versions of the previous scenarios, with larger action modifiers. The learning curves reveal a disproportionate effect of this additional difficulty on the extended methods, being PSL and MSL considerably more affected.

The value distance shows that ASL learned valuable symmetry transformations but not as reliable as in **A2**, resulting in a more asymmetric policy. The average target error confirms this efficiency decline even though the initial symmetry transformation had an average error of 0.503 and, after training, that value dropped to 0.128 on **A2.1** and 0.106 on **A2.2**. As

expected, due to some transformation targets still having a considerable error, the gait was more affected for some goals, resulting in an NSRR imbalance between plane $y=x$ and $y=-x$.

A4

In **A4.1** to **A4.3**, additional weight is placed on the first and second feet, while in **A4.4** to **A4.6**, the extra weight is placed on the first and third feet. This realistic scenario takes advantage of symmetry fitting to adjust the linear imbalance in symmetry transformations, while the non-linear adjustments are handled by PPO. For this reason, in general, ASL learns faster and reaches higher episode returns in the end. The best results were attained for transformations modeled as linear operations of the form $y = mx + b$.

MSL and PSL had similar performances, with the former learning faster in 3 scenarios, while the latter achieved a higher final performance in the last 2 scenarios. As for ASL, the transformation targets standard deviation across 12 instances, averaged over all multipliers and biases, was [0.05,0.06,0.06,0.04,0.13,0.08] for each scenario, indicating that symmetry fitting was consistent in independent optimizations.

A noteworthy result was that simultaneously training on all goals (**A4.1** and **A4.4**) did not appear to harm the final performance. This implies that in some cases, the performance on odd goals actually improved, in comparison with **A4.2** and **A4.5**. The scenario with lowest gain for ASL was **A4.6** in terms of episode return. This might be explained by the value distance plots, since it's the only scenario where ASL does not take the lead, hinting that symmetry fitting did not sufficiently improve results in this configuration. Finally, the NSRR plots show an imbalance towards $y=x$ except in **A4.3** and **A4.6**, since these do not contain any odd goals (where one front leg is required).

A5

A5.1 and **A5.2** are equivalent to **A4.1** and **A4.4**, respectively, except that the policies could only train on the first 4 goals, having to generalize that knowledge to the remaining ones. In theory, the first 4 goals have enough information to learn the linear part of these modifications. However, when training with 4 goals, the policy explores only 4 different gaits, yielding a more biased linear transformation estimate, despite having lower average standard deviation, at [0.03,0.03] per scenario. Regardless of the overall loss of performance in comparison with **A4**, ASL generates considerably better policies than MSL or PSL.

A6

In **A6** there are no feet mass modification, but the floor surface is tilted 5 degrees in a specific direction. The results were underwhelming but also though-provoking. For instance, the gait used to go down a small slope is different from the one used to go up, but we expected to find similarities that could be used to linearly model part of that relationship. In fact, the symmetry transformation targets are almost as stable as in **A4**, with an average standard deviation of

[0.06,0.08,0.07,0.06,0.08,0.06]. Moreover, these transformations were not discarded by the policy, as demonstrated by the lower value distance in comparison with other methods. However, in general, the results were mostly on par with MSL and PSL, both in terms of learning speed and final accuracy.

Two potential conclusions can be derived from this outcome. First, the nonlinear part of the symmetric relation can monopolize the optimization, leaving most of the adaptation work to PPO. Second, the benefit of adapting the symmetry transformations in **A6** might be canceled out by the additional variance introduced by modifying such transformations during optimization.

XIV. CONCLUSION

There are multiple approaches to model minimization that are concerned with reducing redundant symmetries. Loss functions are the most versatile way of achieving this objective, due to their ability to represent complex concepts but also because they can directly control the optimization direction by producing a gradient. For actor-critic methods such as PPO, their loss functions can be extended to introduce symmetry concepts that will influence the optimization of the policy and value function.

This work presents two existing symmetry loss functions — Mirror Symmetry Loss (MSL) and Proximal Symmetry Loss (PSL) — extending them with value losses and, for MSL, the capacity to handle involutory transformations, such as most rotations. A novel Adaptive Symmetry Learning (ASL) method is presented, where the main focus is to handle incomplete or inexact symmetry descriptions by learning adaptations. There are multiple sources for potential imperfections, including perturbations in the robot, environment, reward function, or agent (control process).

ASL is composed of a symmetry fitting component and a modular loss function with useful gates to exclude neutral states and disadvantageous updates. While the policy is learning the best action for each state, ASL’s loss function is enforcing a common symmetric linear relation across all states and, at the same time, adapting that same relation to match what the policy is learning. Adapting non-linear relations is also an option, although it can be counterproductive due to the additional learning time. In the end, it is a trade-off between the convergence efficiency of symmetry transformations and the policy itself.

The case study presented in this work explored a four-legged ant model adapted from PyBullet’s AntBulletEnv-v0. This is an interesting model to learn multidirectional locomotion tasks as it admits 7 non-identity symmetry transformations — 4 reflections and 3 rotations. In all the proposed scenarios, vanilla PPO was not enough to learn solid policies. By contrast, PPO+ASL was able to equal or outperform the alternative symmetry-enhanced methods in most situations.

The main strengths that differentiate ASL are its performance in recovering from large linearly modelable perturbations, and generalizing knowledge to hidden symmetric states. The former characteristic was observed in a controlled setting (scenario **A3**) and in a realistic context (**A4**). The ability to

successfully cope with hidden symmetric states was verified in configurations with symmetry fitting (**A5**) and without it (**A1.2**).

ASL was comparable to MSL and PSL in perfectly symmetric and fully observable conditions (**A1.1**), and slightly imperfect models (**A2**). Finally, in an inclined surface (**A6**), ASL exhibited a mixed performance, producing consistent adaptations but not translating that into better episode returns. In conclusion, the advantage of using ASL in relation to other symmetry loss functions depends on the context. However, in general, its efficiency is at least as good as the other methods, being in some circumstances considerably better.

Future research directions encompass automating hyperparameter optimization through meta-learning to mitigate setup complexity, enabling faster results with limited computational resources. Additionally, exploring symmetry perturbations that deteriorate over time as a result of wear and tear on robot components constitutes another promising avenue of investigation. While ASL can accommodate dynamic symmetry relationships without getting stuck in local minima, alternative approaches to PPO should be explored for handling changing environments.

REFERENCES

- [1] H. Weyl, *Symmetry*. Princeton University Press, Princeton, 1952.
- [2] K. Mainzer, *Symmetry and complexity: The spirit and beauty of nonlinear science*. World Scientific, 2005, vol. 51.
- [3] M. Papadatou-Pastou, E. Ntolka, J. Schmitz, M. Martin, M. R. Munafò, S. Ocklenburg, and S. Paracchini, “Human handedness: A meta-analysis.” *Psychological bulletin*, vol. 146, no. 6, p. 481, 2020.
- [4] L.-J. Lin, “Self-improving reactive agents based on reinforcement learning, planning and teaching,” *Machine learning*, vol. 8, no. 3-4, pp. 293–321, 1992.
- [5] M. G. Browne, C. S. Smock, and R. T. Roemmich, “The human preference for symmetric walking often disappears when one leg is constrained,” *The Journal of physiology*, vol. 599, no. 4, pp. 1243–1260, 2021.
- [6] I. Handžić and K. B. Reed, “Perception of gait patterns that deviate from normal and symmetric biped locomotion,” *Frontiers in psychology*, vol. 6, p. 199, 2015.
- [7] B. Ravindran and A. G. Barto, “Symmetries and model minimization in markov decision processes,” University of Massachusetts, USA, Tech. Rep., 2001.
- [8] M. Zinkevich and T. R. Balch, “Symmetry in markov decision processes and its implications for single agent and multiagent learning,” in *Proceedings of the Eighteenth International Conference on Machine Learning*, ser. ICML ’01. San Francisco, CA, USA: Morgan Kaufmann Publishers Inc., 2001, p. 632.
- [9] A. Agostini and E. Celaya, “Exploiting domain symmetries in reinforcement learning with continuous state and action spaces,” in *2009 International Conference on Machine Learning and Applications*. IEEE, 2009, pp. 331–336.
- [10] K. Zeng and M. D. Graham, “Symmetry reduction for deep reinforcement learning active control of chaotic spatiotemporal dynamics,” *Phys. Rev. E*, vol. 104, p. 014210, Jul 2021.
- [11] P. Ildefonso, P. Remédios, R. Silva, M. Vasco, F. S. Melo, A. Paiva, and M. Veloso, “Exploiting symmetry in human robot-assisted dressing using reinforcement learning,” in *Progress in Artificial Intelligence: 20th EPIA Conference on Artificial Intelligence, EPIA 2021, Virtual Event, September 7–9, 2021, Proceedings 20*. Springer, 2021, pp. 405–417.
- [12] D. Surovik, K. Wang, M. Vespignani, J. Bruce, and K. E. Bekris, “Adaptive tensegrity locomotion: Controlling a compliant icosahedron with symmetry-reduced reinforcement learning,” *The International Journal of Robotics Research*, 2019.
- [13] Z. Xie, P. Clary, J. Dao, P. Morais, J. Hurst, and M. van de Panne, “Learning locomotion skills for cassie: Iterative design and sim-to-real,” in *Proceedings of the Conference on Robot Learning*, ser. Proceedings of Machine Learning Research, L. P. Kaelbling, D. Kragic, and K. Sugiura, Eds., vol. 100. PMLR, 2020, pp. 317–329.

- [14] A. Hereid, C. M. Hubicki, E. A. Cousineau, and A. D. Ames, “Dynamic humanoid locomotion: A scalable formulation for HZD gait optimization,” *IEEE Transactions on Robotics*, vol. 34, no. 2, pp. 370–387, 2018.
- [15] X. B. Peng, G. Berseth, K. Yin, and M. van de Panne, “Deeploco: Dynamic locomotion skills using hierarchical deep reinforcement learning,” *ACM Trans. on Graphics (Proc. SIGGRAPH 2017)*, vol. 36, no. 4, 2017.
- [16] R. van Bree, “Data augmentation for regularizing learned world models in reinforcement learning,” Master’s thesis, University of Twente, 2021.
- [17] Y. Lin, J. Huang, M. Zimmer, Y. Guan, J. Rojas, and P. Weng, “Invariant transform experience replay: Data augmentation for deep reinforcement learning,” *IEEE Robotics and Automation Letters*, vol. 5, no. 4, pp. 6615–6622, 2020.
- [18] F. Abdolhosseini, H. Y. Ling, Z. Xie, X. B. Peng, and M. van de Panne, “On learning symmetric locomotion,” in *Motion, Interaction and Games*, 2019, pp. 1–10.
- [19] S. Mishra, A. Abdolmaleki, A. Guez, P. Trochim, and D. Precup, “Augmenting learning using symmetry in a biologically-inspired domain,” arXiv preprint arXiv:1910.00528, 2019.
- [20] D. Silver, A. Huang, C. J. Maddison, A. Guez, L. Sifre, G. Van Den Driessche, J. Schrittwieser, I. Antonoglou, V. Panneershelvam, M. Lanctot *et al.*, “Mastering the game of go with deep neural networks and tree search,” *Nature*, vol. 529, no. 7587, pp. 484–489, 2016.
- [21] E. van der Pol, D. E. Worrall, H. van Hoof, F. A. Oliehoek, and M. Welling, “MDP homomorphic networks: Group symmetries in reinforcement learning,” in *Advances in Neural Information Processing Systems*, 2020.
- [22] A. Bhattacharya, M. Mattheakis, and P. Protopoulos, “Encoding involuntary invariances in neural networks,” in *2022 International Joint Conference on Neural Networks (IJCNN)*, 2022.
- [23] A. K. Mondal, P. Nair, and K. Siddiqi, “Group equivariant deep reinforcement learning,” arXiv preprint arXiv:2007.03437, 2020.
- [24] S. Ravanbakhsh, J. Schneider, and B. Póczos, “Equivariance through parameter-sharing,” in *International conference on machine learning*. PMLR, 2017, pp. 2892–2901.
- [25] A. Sannai, Y. Takai, and M. Cordonnier, “Universal approximations of permutation invariant/equivariant functions by deep neural networks,” arXiv preprint arXiv:1903.01939, 2019.
- [26] T. Cohen and M. Welling, “Group equivariant convolutional networks,” in *International conference on machine learning*. PMLR, 2016, pp. 2990–2999.
- [27] A. Mahajan and T. Tulabandhula, “Symmetry detection and exploitation for function approximation in deep RL,” in *Proceedings of the 16th Conference on Autonomous Agents and MultiAgent Systems*, ser. AAMAS ’17. Richland, SC: International Foundation for Autonomous Agents and Multiagent Systems, 2017, p. 1619–1621.
- [28] A. Mahajan and T. Tulabandhula, “Symmetry learning for function approximation in reinforcement learning,” arXiv preprint arXiv:1706.02999, 2017.
- [29] C. J. Watkins and P. Dayan, “Q-learning,” *Machine learning*, vol. 8, no. 3-4, pp. 279–292, 1992.
- [30] W. Yu, G. Turk, and C. K. Liu, “Learning symmetric and low-energy locomotion,” *ACM Transactions on Graphics (TOG)*, vol. 37, no. 4, Jul. 2018.
- [31] M. Kasaei, M. Abreu, N. Lau, A. Pereira, and L. P. Reis, “A CPG-based agile and versatile locomotion framework using proximal symmetry loss,” arXiv preprint arXiv:2103.00928, 2021.
- [32] P. Dhariwal, C. Hesse, O. Klimov, A. Nichol, M. Plappert, A. Radford, J. Schulman, S. Sidor, Y. Wu, and P. Zhokhov, “OpenAI Baselines,” <https://github.com/openai/baselines>, 2017.
- [33] A. Hill, A. Raffin, M. Ernestus, A. Gleave, A. Kanervisto, R. Traore, P. Dhariwal, C. Hesse, O. Klimov, A. Nichol, M. Plappert, A. Radford, J. Schulman, S. Sidor, and Y. Wu, “Stable baselines,” <https://github.com/hill-a/stable-baselines>, 2018.
- [34] R. McWeeny, *Symmetry: an introduction to group theory and its applications*. Pergamon Press, MacMillan, New York, 1963.
- [35] F. M. Jaeger, *Lectures on the principle of symmetry and its applications in all natural sciences*. Elsevier, Amsterdam, 1917.
- [36] B. Everitt, *The Cambridge dictionary of statistics*, 4th ed. Cambridge, UK: Cambridge University Press, 2010.
- [37] J. Schulman, S. Levine, P. Abbeel, M. Jordan, and P. Moritz, “Trust region policy optimization,” in *International conference on machine learning*. PMLR, 2015, pp. 1889–1897.
- [38] D. P. Kingma and J. Ba, “Adam: A method for stochastic optimization,” in *3rd International Conference on Learning Representations (ICLR)*, Y. Bengio and Y. LeCun, Eds., San Diego, CA, USA, 2015.
- [39] J. Schulman, F. Wolski, P. Dhariwal, A. Radford, and O. Klimov, “Proximal policy optimization algorithms,” arXiv preprint arXiv:1707.06347, 2017.
- [40] E. Coumans and Y. Bai, “Pybullet, a python module for physics simulation for games, robotics and machine learning,” <http://pybullet.org>, 2016–2022.
- [41] A. Raffin, A. Hill, A. Gleave, A. Kanervisto, M. Ernestus, and N. Dormann, “Stable-Baselines3: Reliable reinforcement learning implementations,” *Journal of Machine Learning Research*, vol. 22, no. 268, pp. 1–8, 2021. [Online]. Available: <http://jmlr.org/papers/v22/20-1364.html>
- [42] E. Logan, I. Andrew, S. Shibani, T. Dimitris, J. Firdaus, R. Larry, and M. Aleksander, “Implementation matters in deep rl: A case study on ppo and trpo,” in *International Conference on Learning Representations*, 2019.
- [43] M. Andrychowicz, A. Raichuk, P. Stańczyk, M. Orsini, S. Girgin, R. Marinier, L. Hussenot, M. Geist, O. Pietquin, M. Michalski *et al.*, “What matters in on-policy reinforcement learning? a large-scale empirical study,” arXiv preprint arXiv:2006.05990, 2020.
- [44] A. Raffin, “RL baselines3 zoo,” <https://github.com/DLR-RM/rl-baselines3-zoo>, 2020.

APPENDIX A SYMMETRY TRANSFORMATIONS

yz-plane	action indices	2 3 0 1 6 7 4 5	obs. indices																									
	action multipliers	-1 -1 -1 -1 -1 -1 -1 -1	obs. multipliers																									
0	1	2	3	4	5	6	7	12	13	14	15	8	9	10	11	20	21	22	23	16	17	18	19	25	24	27	26	
1	1	-1	-1	1	1	1	-1	-1	-1	-1	-1	-1	-1	-1	-1	-1	-1	-1	-1	-1	-1	-1	-1	-1	1	1	1	1

y=x plane	action indices	0 1 6 7 4 5 2 3	obs. indices																									
	action multipliers	-1 1 -1 -1 -1 1 -1 -1	obs. multipliers																									
0	2	1	4	3	5	7	6	8	9	10	11	20	21	22	23	16	17	18	19	12	13	14	15	24	27	26	25	
1	1	1	1	1	1	-1	-1	-1	-1	1	1	-1	-1	-1	-1	-1	-1	-1	-1	-1	-1	-1	-1	-1	1	1	1	1

y=-x plane	action indices	4 5 2 3 0 1 6 7	obs. indices																								
	action multipliers	-1 -1 -1 1 -1 -1 -1 1	obs. multipliers																								
0	2	1	4	3	5	7	6	16	17	18	19	12	13	14	15	8	9	10	11	20	21	22	23	26	25	24	27
1	-1	-1	-1	-1	1	1	1	-1	-1	-1	-1	-1	-1	-1	-1	-1	-1	-1	-1	-1	-1	-1	-1	1	1	1	1

z-axis 90°	action indices	6 7 0 1 2 3 4 5	obs. indices																								
	action multipliers	1 1 1 -1 1 1 1 -1	obs. multipliers																								
0	2	1	4	3	5	7	6	20	21	22	23	8	9	10	11	12	13	14	15	16	17	18	19	27	24	25	26
1	1	-1	-1	1	1	-1	-1	1	1	1	1	1	-1	-1	1	1	1	1	1	1	1	1	-1	-1	1	1	1

z-axis 180°	action indices	4 5 6 7 0 1 2 3	obs. indices																								
	action multipliers	1 -1 1 -1 1 -1 1 -1	obs. multipliers																								
0	1	2	3	4	5	6	7	16	17	18	19	20	21	22	23	8	9	10	11	12	13	14	15	26	27	24	25
1	-1	-1	-1	-1	1	1	-1	1	1	-1	-1	1	1	-1	-1	1	1	-1	-1	1	1	-1	-1	1	1	1	1

z-axis 270°	action indices	2 3 4 5 6 7 0 1	obs. indices																								
	action multipliers	1 -1 1 1 1 -1 1 1	obs. multipliers																								
0	2	1	4	3	5	7	6	12	13	14	15	16	17	18	19	20	21	22	23	8	9	10	11	25	26	27	24
1	-1	1	1	-1	1	1	-1	1	1	-1	-1	1	1	1	1	-1	-1	1	1	1	1	1	1	1	1	1	1

Fig. 20. Remaining symmetry transformation for AntBulletEnv-v0, as a complement to Fig. 15.

APPENDIX B EVALUATION HYPERPARAMETERS

TABLE VIII
SCENARIO A1.1 — ASL HYPERPARAMETERS

Method	Symbol	Short Description	Value
all	TS	total time steps	4×10^6
ASL	w_π	policy sym. loss weight	0.05
ASL	$H_U, H_F, g(a)$ form	symmetry fitting	Disabled
ASL	k_s	max. distribution shift	0.3
ASL	$k_d[\text{reflec}]$	dead zone (sym. plane)	0.1
MSL	w_π	policy sym. loss weight	10
PSL	w_π	policy sym. loss weight	0.008

TABLE IX
SCENARIO A1.2 — ASL HYPERPARAMETERS

Method	Symbol	Short Description	Value
all	TS	total time steps	4×10^6
ASL	w_π	policy sym. loss weight	0.25
ASL	$H_U, H_F, g(a)$ form	symmetry fitting	Disabled
ASL	k_s	max. distribution shift	1
ASL	$k_d[\text{reflec}]$	dead zone (sym. plane)	0.2
ASL	k_v	value gate factor	Disabled
MSL	w_π	policy sym. loss weight	10
PSL	w_π	policy sym. loss weight	0.08

TABLE X
SCENARIO A2.1 — ASL HYPERPARAMETERS

Method	Symbol	Short Description	Value
all	TS	total time steps	4×10^6
ASL	w_π	policy sym. loss weight	0.05
ASL	k_s	max. distribution shift	0.3
ASL	$k_d[\text{reflec}]$	dead zone (sym. plane)	0.1
ASL	$g(a)$ form	function form of $g(a)$	$y = mx$
MSL	w_π	policy sym. loss weight	3
PSL	w_π	policy sym. loss weight	0.003

TABLE XI
SCENARIO A2.2 — ASL HYPERPARAMETERS

Method	Symbol	Short Description	Value
all	TS	total time steps	4×10^6
ASL	w_π	policy sym. loss weight	0.05
ASL	k_s	max. distribution shift	0.2
ASL	$k_d[\text{reflec}]$	dead zone (sym. plane)	0.1
ASL	$g(a)$ form	function form of $g(a)$	$y = mx$
MSL	w_π	policy sym. loss weight	2
PSL	w_π	policy sym. loss weight	0.001

TABLE XII
SCENARIO A3.1 — ASL HYPERPARAMETERS

Method	Symbol	Short Description	Value
all	TS	total time steps	5×10^6
ASL	w_π	policy sym. loss weight	0.1
ASL	k_s	max. distribution shift	0.5
ASL	$k_d[\text{reflec}]$	dead zone (sym. plane)	0.1
ASL	$g(a)$ form	function form of $g(a)$	$y = mx$
MSL	w_π	policy sym. loss weight	1
PSL	w_π	policy sym. loss weight	0.001

TABLE XIII
SCENARIO A3.2 — ASL HYPERPARAMETERS

Method	Symbol	Short Description	Value
all	TS	total time steps	5×10^6
ASL	w_π	policy sym. loss weight	0.1
ASL	k_s	max. distribution shift	0.25
ASL	$k_d[\text{reflec}]$	dead zone (sym. plane)	0.1
ASL	$g(a)$ form	function form of $g(a)$	$y = mx$
MSL	w_π	policy sym. loss weight	0.1
PSL	w_π	policy sym. loss weight	0.001

TABLE XIV
SCENARIO A4.1 — ASL HYPERPARAMETERS

Method	Symbol	Short Description	Value
all	TS	total time steps	5×10^6
ASL	w_π	policy sym. loss weight	0.1
ASL	k_s	max. distribution shift	0.1
ASL	$k_d[\text{reflec}]$	dead zone (sym. plane)	0.2
ASL	$g(a)$ form	function form of $g(a)$	$y = mx + b$
MSL	w_π	policy sym. loss weight	0.05
PSL	w_π	policy sym. loss weight	0.0005

TABLE XV
SCENARIO A4.2 — ASL HYPERPARAMETERS

Method	Symbol	Short Description	Value
all	TS	total time steps	5×10^6
ASL	w_π	policy sym. loss weight	0.1
ASL	k_s	max. distribution shift	0.1
ASL	$k_d[\text{reflec}]$	dead zone (sym. plane)	0.2
ASL	$g(a)$ form	function form of $g(a)$	$y = mx + b$
MSL	w_π	policy sym. loss weight	0.05
PSL	w_π	policy sym. loss weight	0.001

TABLE XVI
SCENARIO A4.3 — ASL HYPERPARAMETERS

Method	Symbol	Short Description	Value
all	TS	total time steps	5×10^6
ASL	w_π	policy sym. loss weight	0.1
ASL	k_s	max. distribution shift	0.1
ASL	$k_d[\text{reflec}]$	dead zone (sym. plane)	0.2
ASL	$g(a)$ form	function form of $g(a)$	$y = mx + b$
MSL	w_π	policy sym. loss weight	0.05
PSL	w_π	policy sym. loss weight	0.001

TABLE XVII
SCENARIO A4.4 — ASL HYPERPARAMETERS

Method	Symbol	Short Description	Value
all	TS	total time steps	5×10^6
ASL	w_π	policy sym. loss weight	0.1
ASL	k_s	max. distribution shift	0.1
ASL	$k_d[\text{reflec}]$	dead zone (sym. plane)	0.2
ASL	$g(a)$ form	function form of $g(a)$	$y = mx + b$
MSL	w_π	policy sym. loss weight	0.05
PSL	w_π	policy sym. loss weight	0.001

TABLE XVIII
SCENARIO A4.5 — ASL HYPERPARAMETERS

Method	Symbol	Short Description	Value
all	TS	total time steps	5×10^6
ASL	w_π	policy sym. loss weight	0.05
ASL	k_s	max. distribution shift	0.02
ASL	$k_d[\text{reflec}]$	dead zone (sym. plane)	0.2
ASL	$g(a)$ form	function form of $g(a)$	$y = mx + b$
MSL	w_π	policy sym. loss weight	0.0005
PSL	w_π	policy sym. loss weight	0.0005

TABLE XIX
SCENARIO A4.6 — ASL HYPERPARAMETERS

Method	Symbol	Short Description	Value
all	TS	total time steps	5×10^6
ASL	w_π	policy sym. loss weight	0.05
ASL	k_s	max. distribution shift	0.05
ASL	$k_d[\text{reflec}]$	dead zone (sym. plane)	0.2
ASL	$g(a)$ form	function form of $g(a)$	$y = mx + b$
MSL	w_π	policy sym. loss weight	0.05
PSL	w_π	policy sym. loss weight	0.001

TABLE XX
SCENARIO A5.1 — ASL HYPERPARAMETERS

Method	Symbol	Short Description	Value
all	TS	total time steps	5×10^6
ASL	w_π	policy sym. loss weight	0.2
ASL	k_s	max. distribution shift	0.4
ASL	$k_d[\text{reflec}]$	dead zone (sym. plane)	0.2
ASL	$g(a)$ form	function form of $g(a)$	$y = mx + b$
MSL	w_π	policy sym. loss weight	0.05
PSL	w_π	policy sym. loss weight	0.002

TABLE XXI
SCENARIO A5.2 — ASL HYPERPARAMETERS

Method	Symbol	Short Description	Value
all	TS	total time steps	5×10^6
ASL	w_π	policy sym. loss weight	0.2
ASL	k_s	max. distribution shift	0.4
ASL	$k_d[\text{reflec}]$	dead zone (sym. plane)	0.2
ASL	$g(a)$ form	function form of $g(a)$	$y = mx + b$
MSL	w_π	policy sym. loss weight	0.02
PSL	w_π	policy sym. loss weight	0.004

TABLE XXII
SCENARIO A6 — ASL HYPERPARAMETERS

Method	Symbol	Short Description	Value
all	TS	total time steps	5×10^6
ASL	w_π	policy sym. loss weight	0.05
ASL	k_s	max. distribution shift	0.1
ASL	$k_d[\text{reflec}]$	dead zone (sym. plane)	0.2
ASL	$g(a)$ form	function form of $g(a)$	$y = mx + b$
MSL	w_π	policy sym. loss weight	0.01
PSL	w_π	policy sym. loss weight	0.0005

APPENDIX C
EVALUATION RESULTS

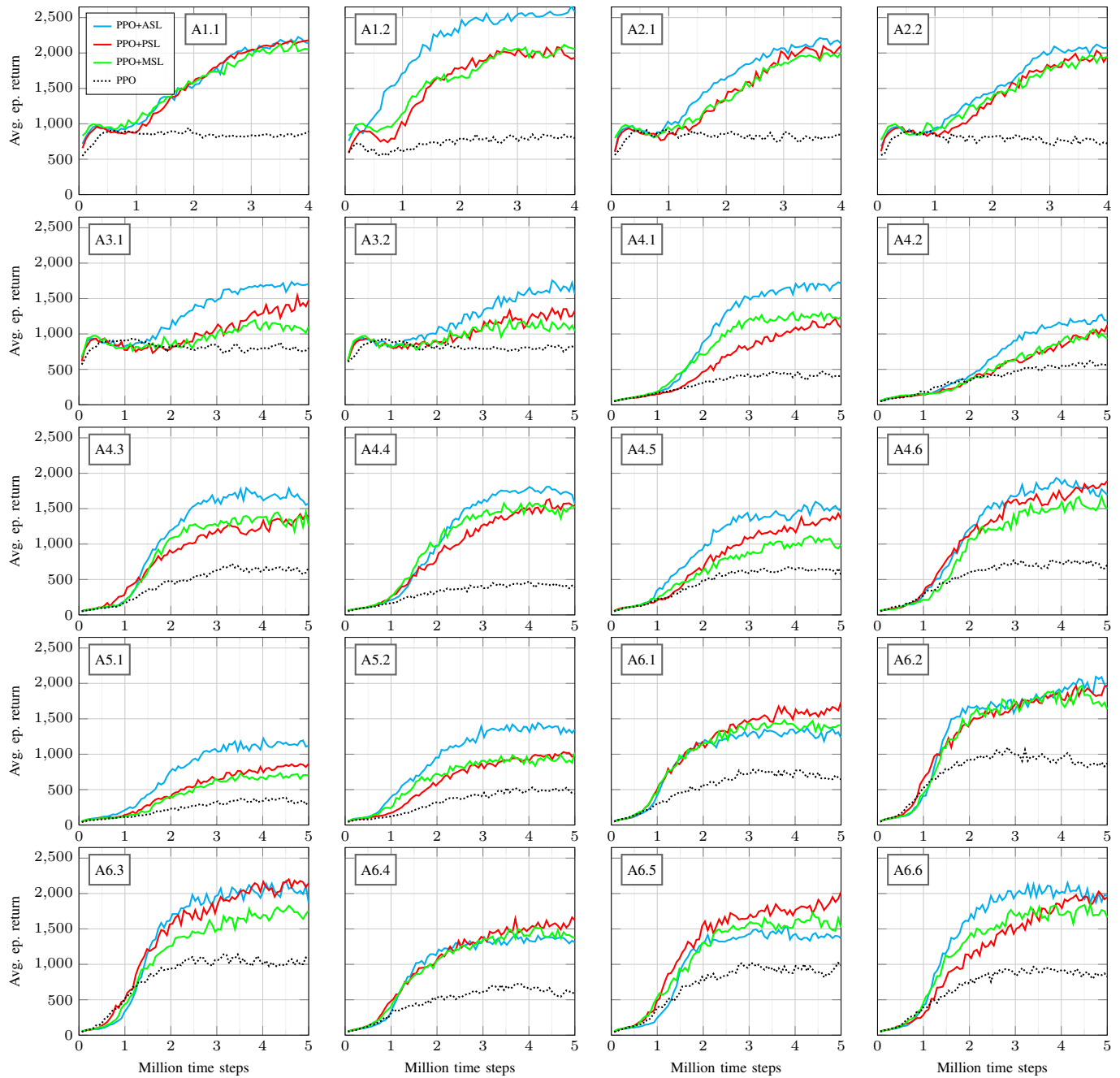


Fig. 21. Average learning curves for a batch of 12 instances per algorithm, per scenario. The deterministic neural network output of each policy was evaluated every 15 iterations, i.e., every 61440 time steps. The evaluated algorithms are: PPO without extensions (dotted black), PPO with Adaptive Symmetry Learning (solid blue), PPO with Proximal Symmetry Learning (solid red), PPO with generalized Mirror Symmetry Loss (solid green).

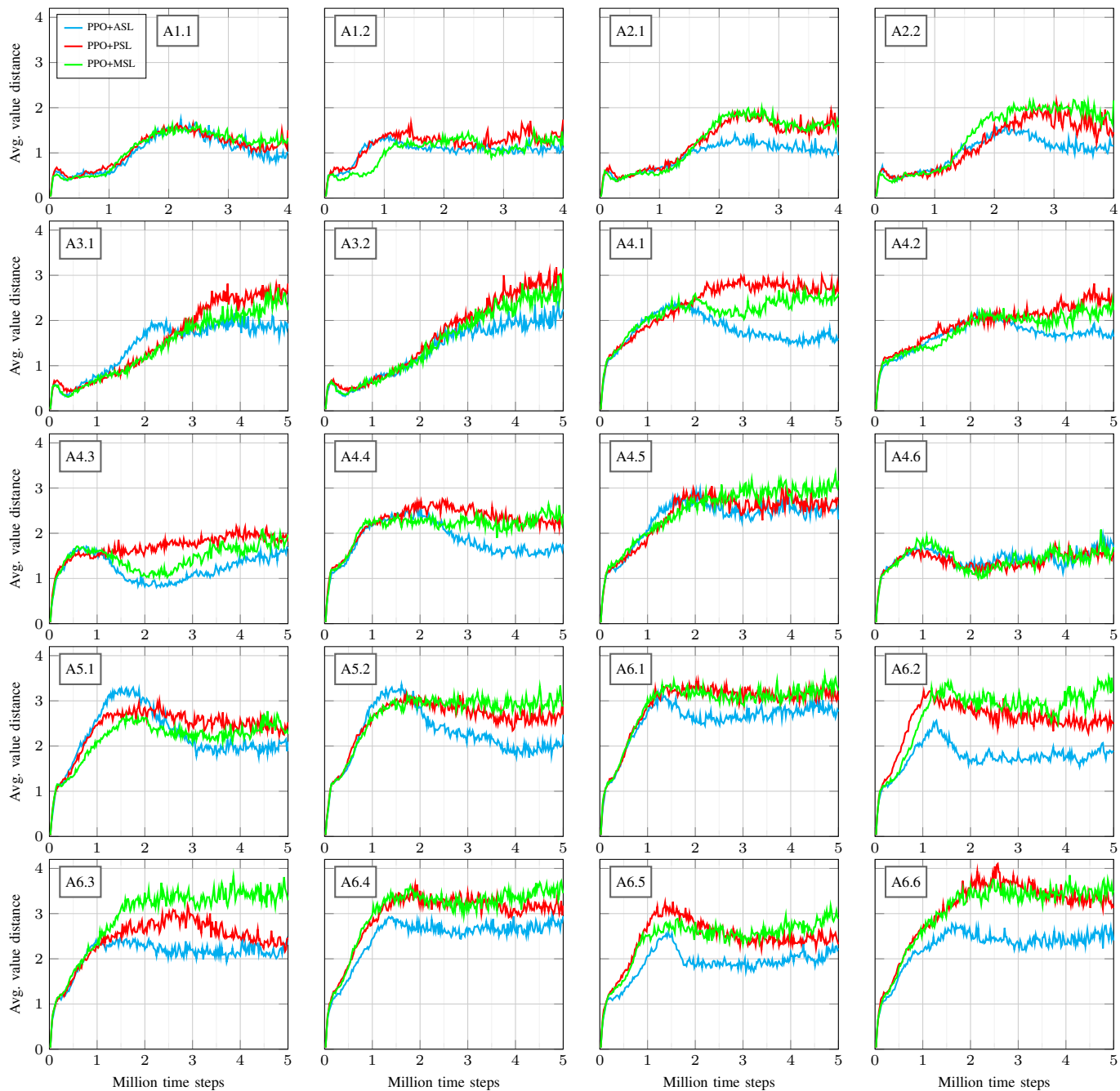


Fig. 22. Average absolute difference between the value estimates of the explored state and the corresponding symmetric state. Each data point is obtained every 5 iterations and is an average of all the explored states in the last iteration, averaged over 12 instances. The evaluated algorithms are: PPO with Adaptive Symmetry Learning (blue), PPO with Proximal Symmetry Learning (red), PPO with generalized Mirror Symmetry Loss (green).

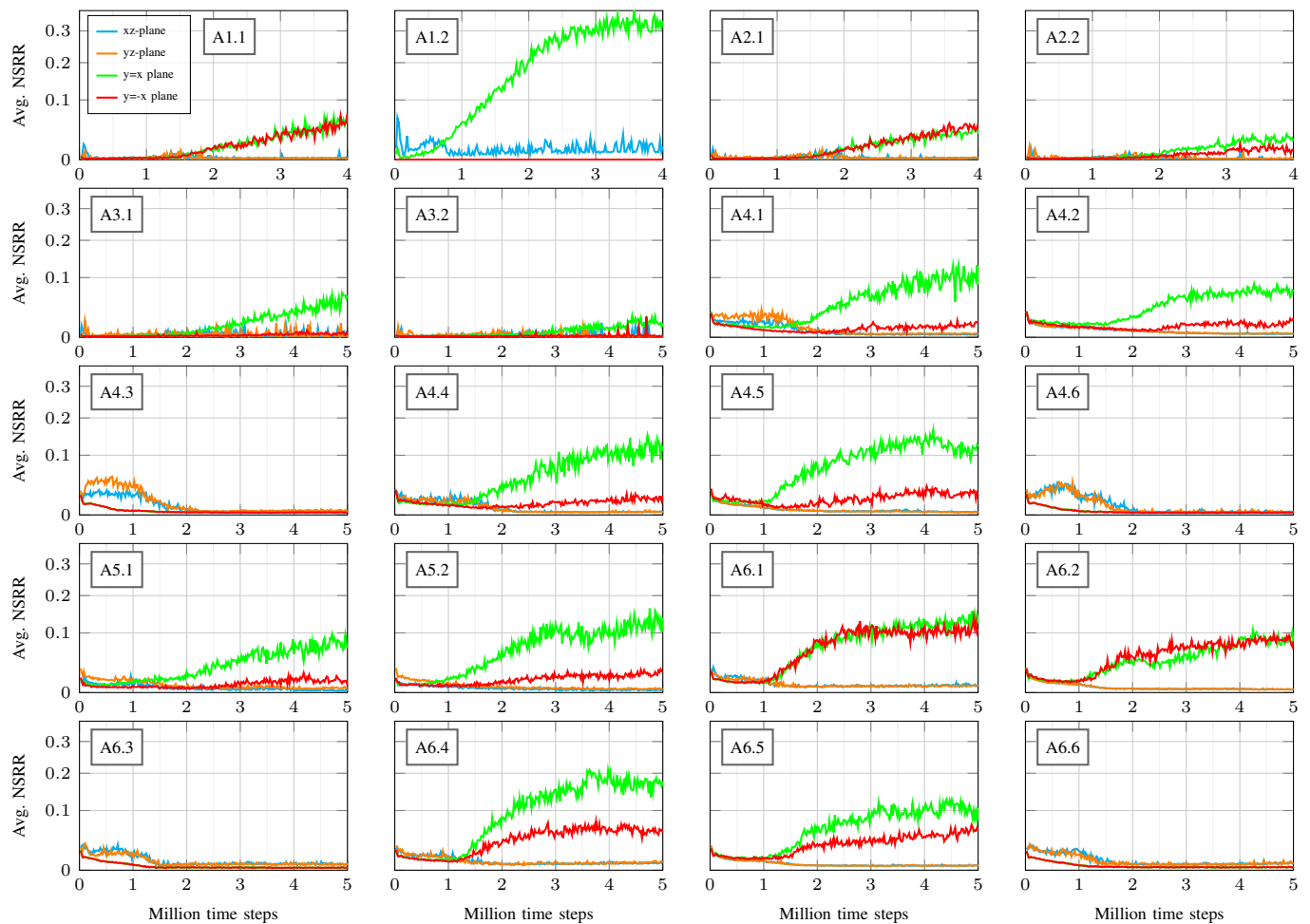


Fig. 23. Average neutral state rejection ratio (NSRR), i.e. ratio of states that were rejected by the Adaptive Symmetry Learning algorithm (see Section IX-B). Each data point is an average of 12 instances per symmetry plane, per scenario, obtained every 5 iterations. The evaluated symmetry planes are: xz-plane (blue), yz-plane (orange), y=x plane (green), y=-x plane (red).

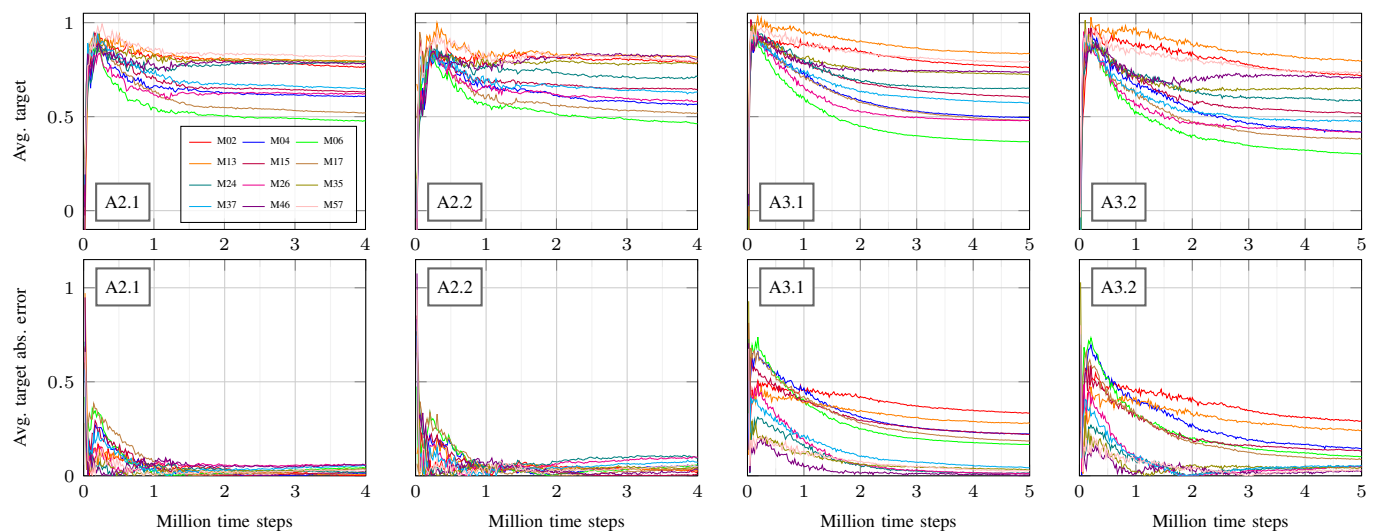


Fig. 24. Average symmetry transformation (multiplier) target (above) and the respective absolute error (below) for the Adaptive Symmetry Learning algorithm. Each data point is an average of 12 instances per pair of symmetric action dimensions ($m_{0 \rightarrow 2}$ to $m_{5 \rightarrow 7}$), per scenario (A2 and A3), obtained every 5 iterations.

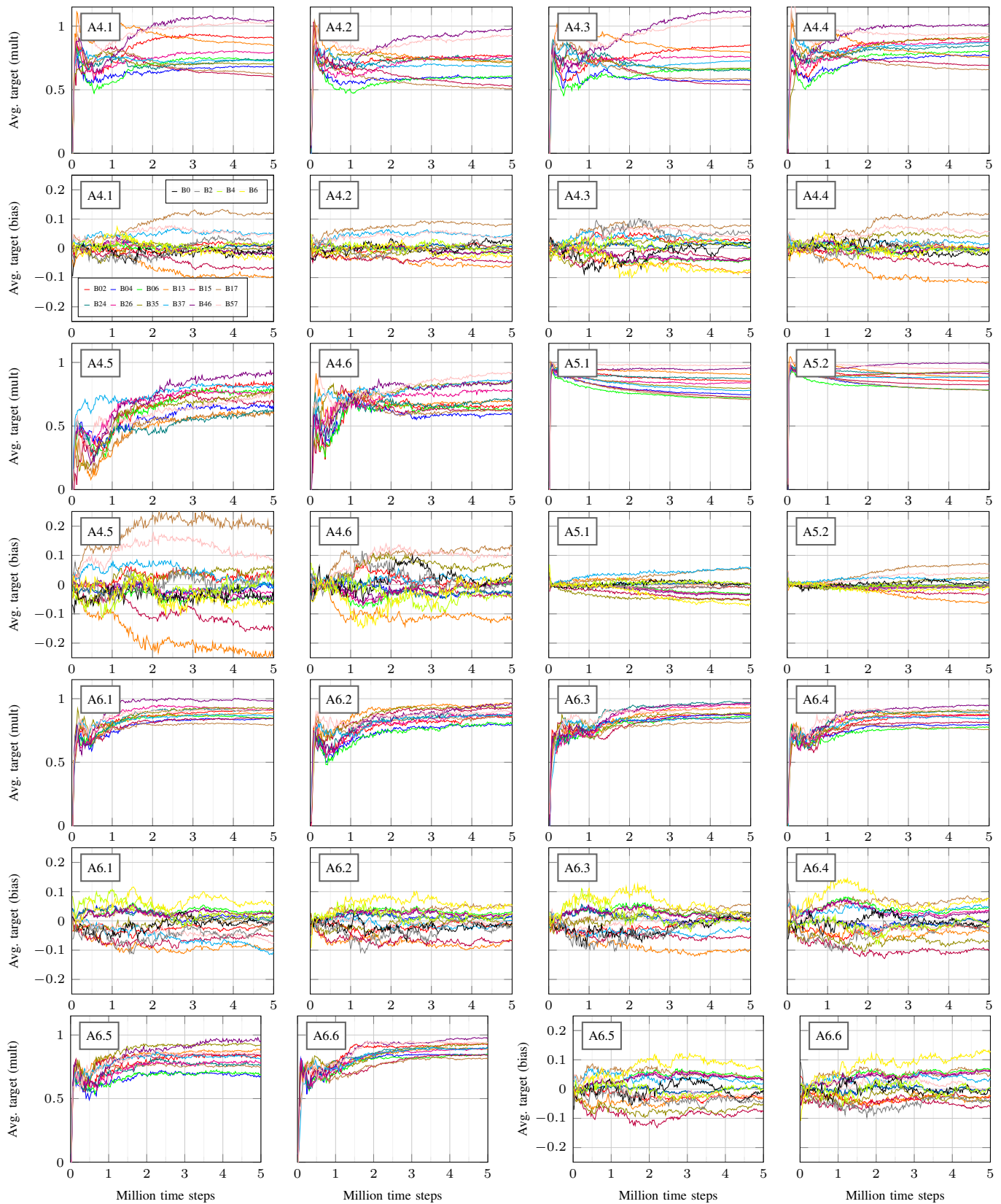


Fig. 25. Average symmetry transformation (multiplier/bias) targets for the Adaptive Symmetry Learning algorithm. Each data point is an average of 12 instances per pair of symmetric action dimensions ($m_{0 \rightarrow 2}$ to $m_{5 \rightarrow 7}$ and $b_{0 \rightarrow 2}$ to $b_{5 \rightarrow 7}$) and reflexive relations/singles (b_0 , b_2 , b_4 and b_6), per scenario (**A4** to **A6**), obtained every 5 iterations.